PIEZOELECTRIC MICROPUMP FOR DRUG DELIVERY APPLICATION

by

MITESHKUMAR S JOSHI

Presented to the Faculty of the Graduate School of

The University of Texas at Arlington in Partial Fulfillment

of the Requirements

for the Degree of

MASTER OF SCIENCE IN MATERIALS SCIENCE AND ENGINEERING

THE UNIVERSITY OF TEXAS AT ARLINGTON

August 2005

ACKNOWLEDGEMENTS

It’s a great pleasure to acknowledge the people who have been helping me during this work.

First of all I would like to express my sincerest thanks to my advisor Dr. Shashank Priya for his constant support, encouragement and guidance. Without his support and guidance I could not have completed this work. I am indebted to him for changing my research attitude and showing me the right path. He taught me some fundamental principles of life that made me a better human being. I am very grateful to Dr. Priya for giving me this wonderful opportunity to improve my academics and personal skills.

I am very thankful to Dr. Pranesh Aswath for his constant encouragement and guidance and for giving me the chance to start the work in Dr. Priya’s group.

I am very grateful to my lab mates Rashed and Vaneet. Rashed taught me the ceramic processing. I am so thankful to Anurag, Krupal and all my lab mates for helping me whenever I needed. I also thank Jimmy for doing the machining work for me quickly.

I cannot express my gratitude for my parents in words. I am indebted to them for the sacrifices they made throughout my education and particularly to send me for higher studies. Without their everlasting love and support I couldn’t have done this. I

am very thankful to my sister for always being with me and giving me the motivation to go for higher studies.

21 JULY,2005

ABSTRACT

PIEZOELECTRIC MICROPUMP FOR DRUG
DELIVERY APPLICATION

Publication No. ______

Miteshkumar S Joshi, MS

The University of Texas at Arlington, 2005

Supervising Professor: Dr. Shashank Priya

Bending type actuators providing high displacement (~1mm) with low blocking force (~0.5N) and the stack actuators providing low displacement (~1μm) with high blocking force (~1kN) represent the extreme ends of the current piezoelectric actuation technology. In the intermediate range there is deficiency of the actuator designs that provide high displacement with high blocking force in low frequency range of ~2 kHz. This thesis addresses this issue and describes a metal-ceramic actuator design that exhibits high displacement with high blocking force. The structure consist of a piezoelectric bar poled along the length and metal caps were attached to the two

opposite major faces of the bar bounded by steel blocks. The piezoelectric bar is multilayered for operating at low driving voltages.

Extensive FEM analysis using ATILA was conducted to optimize the dimensions of the actuator. FEM results showed that the flextensional mode for actuator of dimension 7x7x40 mm^3 occurs at low frequency of 2.175 kHz. The maximum displacement of about 15 μm was found at driving voltage of 8.5 V. It was observed that by changing the actuator parameters, cavity depth and cap thickness the resonance frequency can be shifted to desired frequency range. These numbers showed that as an actuator, the proposed design has the potential for meeting the high displacement – high blocking force requirement in the low frequency range.

Based on FEM analysis the optimized actuator design was fabricated. A PZT based composition corresponding to $0.98Pb(Zr_{0.52}Ti_{0.48})O_3 + 0.01Nb_2O_5 + 0.01PbO$ was synthesized to fabricate the active actuation component. The fabricated actuator was characterized for impedance, piezoelectric constant and displacement. The results were found to be consistent with the FEM analysis.

As an application this actuator was found suitable for micropump for being used in the controlled drug delivery application. The piezoelectric actuator is used to drive the micropump. Piezoelectric driving mechanism is suitable in this application because it has fast response and operates at low voltages. The designed pump is a valveless diffuser/nozzle pump. It utilizes the property of diffuser that it has less restriction to flow in one direction than in the nozzle direction. The pump operates in two modes:

Pump mode and Supply mode. The characteristics of the pump can be controlled by changing either the applied voltage or the input frequency.

TABLE OF CONTENTS

LIST OF ILLUSTRATIONS

LIST OF TABLES

CHAPTER 1

INTRODUCTION

Significant advances in smart material actuators have taken place in the past decade. The large appeal of using smart material actuators stems from their high mechanical energy density. However, all smart material actuators generally have at least one shortcoming involving either mechanical stroke or displacement. The aim of research is to build an actuator that can generate high displacement and force in a broad frequency range while requiring small electrical power.

The primary design parameters that characterize the authority of any linear actuator are displacement, force, frequency, size, weight, and electrical input power. Most actuators usually perform well in some of these categories. However, design limitation exists for achieving the optimum response in all the categories. An extension of the design envelope is required to accommodate new composite structures.

Smart material actuators have been heavily researched in the past decade because of their high power density as compared with conventional actuators. The most common smart materials used in actuator are piezoelectric, magnetostrictive and shape memory alloy. For example, smart material actuators have 100 to 1000 times as much deliverable mechanical work per unit volume (energy change) and 10 times as much energy per mass as conventional (i.e., electromagnetic, hydraulic or pneumatic) actuators [1]. Smart material actuators are being investigated for use in a variety of areas, including aeroelastic vibration control [2-4], active structural acoustic control [5-7], shape control of surfaces [8-9], flow control of fluids [10-11], and many other applications [12]. Smart actuators utilize energy in the form of heat, light, electric field or magnetic field to generate displacement or force.

SMA generates large strain when temperature changes due to different coefficient of thermal expansion. However, it is difficult to manufacture SMA material and available shapes are limited to long thin wire and bands. Magnetostrictive actuators require large heavy magnets to drive them, have limited band width, and non linear coupling between magnetic field and strain. Piezoelectric actuators overcome all these drawbacks. They provide fast response, large bandwidth and are readily available in various shape and size.

1.1 Types of Actuators

A piezoelectric actuator converts the electrical signal into precisely controlled physical displacement or force. Piezoelectric actuator can be designed to operate in different vibration modes and based on the working mode they are classified as axial, transverse, shear and flexional actuators.

(a) Axial actuator: It operates in d_{33} mode. Electric field is applied in the direction parallel to the poling direction of the piezoelectric ceramic element, and the response is also in the same direction. The ceramic element progressively extends in height as voltage is increased.

(b) Transverse actuator: It operates in the d_{31} mode. Electric field is applied in the direction of piezoelectric ceramic but the response is perpendicular to the direction of polarization. The ceramic element progressively shortens in length as voltage is increased.

(c) Flextensional actuator: It operates in d_{31} mode but its flexible construction makes it capable of significantly larger movement. The amplification mechanisms are of three types.

(1) Internally amplified actuators: It uses the internal piezoelectric strain to induce actuation motion. Bilaminar actuators are typical flextensional actuators. Here two thin piezoelectric ceramic strips or plates are bonded together with polarization direction along thickness direction and connected in parallel. When voltage is applied one layer expands the other contracts, causing the actuator to bend. It gives quadratic amplification of actuator stroke as a function of length.

Unimorph actuator consists of a composite beam, plate or disk with one active layer and one inactive layer or substrate. These unimorph actuators are prestressed either by chemically reducing one side or by high temperature bonding with metal and subsequent cooling to room temperature. RAINBOWS [13], CERAMBOW [14], THUNDER [15] are such unimorph actuators. Other configuration is called building block actuators. It consists of number of small actuators units connected in series or parallel to form larger arrayed actuation system with improved performance, e.g. C-Block actuator [16].

(2) Externally amplified actuator: These actuators use an external mechanism to increase the output deflection. These external mechanisms can be mechanical, hydraulic or other novel kinematic mechanisms. Mechanical amplification scheme utilizing lever arm has a flexure hinged mechanism. Piezoelectric hydraulic actuator uses the displacement response of piezoelectric actuators for hydraulic means [17-18]. A typical piezohydraulic amplifier consists of a piezoceramic stack, an input and output piston, and some type of hydraulic fluid. Transmission ratios of up to 100 are possible using the piezohydralic amplifiers. Other mechanical amplified flextensional actuators are “moonie” and “cymbal”, [19-21]. Here a piezoelectric ceramic disk or stack is sandwiched between two end caps having shallow cavities. Displacement of stack or disk flexes the end caps, producing an increased deflection. The displacement output can be optimized by changing the cavity diameter and depth, metal cap material, metal cap thickness and ceramic thickness.

(3) Frequency leveraged actuators: The strain output from actuators is increased by using the frequency performance of the piezoelectric material to rapidly move the actuator in one direction in a series of small steps. This type of actuator architecture trades the speed of the piezoelectric material for infinite stroke, limited only by the actuator track. The first type of actuator to operate using frequency, developed and patented by Burleigh Instruments in the 1970s, is known as the inchworm [22]. It consists of three actuators connected together that actuate in sequence to move the actuator down a rod. Frequency-leveraged actuators have been useful in a number of applications, particularly where fine positioning coupled with long stroke is required.

All these piezoelectric actuators cover a range of stress and displacement as shown in Fig 1.1. An actuator providing higher stress yields lower displacement and vice versa. The requirement of an actuator which can simultaneously provide high stress and displacement in the low frequency range is critical and needs to be addressed. Additionally, the size of the actuator should be as small as possible.

It should be noticed that a special mechanism is required for obtaining resonance frequency in the range ~2 kHz from a reasonable size actuator. For example, the frequency constants of APC 841(hard PZT ceramic) are: N_L(longitudinal mode)~1700, N_T(thickness mode)~2005, N_P(radial mode)~2055. Thus ceramic of size 850 mm will be required to obtain resonance at 2 kHz in longitudinal mode, ceramic of size 1002 mm will be required to obtain resonance at 2 kHz in thickness mode and ceramic of size 1027 mm will be required to obtain resonance at 2 kHz in radial mode respectively [23]. This thesis presents a unique solution for obtaining resonance in the range of ~2 kHz from a ceramic of length ~30 mm.

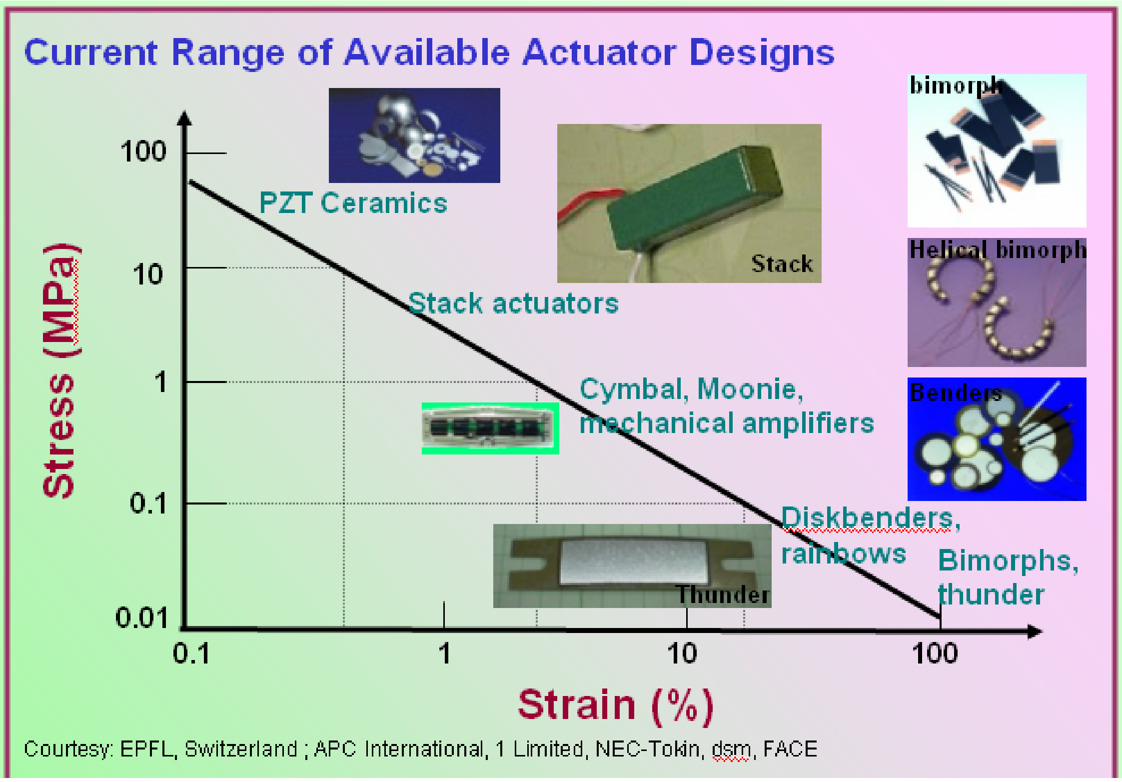

Current Range of Available Actuator Designs

Courtesy: EPFL, Switzerland ; APC International, 1 Limited, NEC-Tokin, dsm, FACE

Fig 1.1 Current range of available actuators

1.2 Micropumps

There is a great and increasing interest in making smaller fluid pumps due to the requirements of the new applications in different chemical, medical and biomedical fields. Theses micropumps are designed to handle small and accurate quantities of fluid. Some of the potential applications are drug delivery for cancer and diabetic patients, controlled fuel delivery in engine and fuel cell, localized cooling in electronics. The first micropump design presented by Spencer et al. in 1978 was based on an actuation of both, the pump diaphragm and valves. Smits carried out initial research and development on micropump using microvalves in 1980s. Based on this idea micromembrane pumps were developed by many researchers [24-26].

Micropumps can be classified in two categories: mechanical pumps with moving parts and non mechanical pumps without moving parts. The mechanical pump utilizes either of the reciprocating, rotary or peristaltic motion [27]. The non mechanical pumps utilize various electric-fluid interaction phenomena to generate forces on fluids. The fluid motion can be induced by the propagating flexural waves and the liquid moves in the direction of wave propagation with the speed proportional to the square of the acoustic amplitude. The electro-osmosis, thermopneumatic, and surface tension are examples of the phenomenon utilized in the design of non mechanical pumps [28-29].

In mechanical pumps with moving parts there are two basic classes: one with inlet and outlet check valves [30] and the other without any valves [26]. The pumps with movable valves have problems of wear and fatigue, pressure loss across valves, valve clogging. Also the operating frequency of pump is limited due to slow actuation of the check valves. The valveless pump eliminates these difficulties and hence has the potential for wide variety of applications. The check valve or diffuser/nozzle and actuator are the key component controlling the maximum flow rate and output pressure of the pump. The maximum output pressure of a micropump directly depends on the force the actuator can deliver.

According to the data from World Health Organization (WHO) for year 2000, numbers of diabetics in USA were about 15 million and 154 million world wide. The estimated increase in the diabetics' population from 1995 to 2025 is shown in Fig 1.1[31]. Among them about 5-10% are classified as type I diabetics (insulin dependent diabetes mellitus) patients, who need insulin injection everyday. The other 90-95% of patients are mainly type II (non-insulin dependent diabetes mellitus). About 40% of type II diabetes patients need insulin injection. The total number of patients needing injection is estimated to be 6.9 million in USA, 16.3 million in Europe and 71.0 million in world wide according to the data from WHO [31]. The general price of an insulin pump system is about $4000, but most of the cost of system and supplies are covered by many health insurance plans in USA [32]. The lifetime of the drug delivery system is estimated to be about 4 years. If 10% of the diabetes patients needing insulin injection use insulin pump as drug delivery system then the market of the pump is roughly $6.9 million per year in USA alone and will be much larger if the other countries are considered.

Table 1.1 Estimated numbers of diabetics in the U.S and World according to WHO [31]

Number of cases (10^6)	1995	1997	2000	2025
U.S	13.8	14.3	15.0	21.8
Europe	33.0	33.9	35.4	47.7
World	135.2	142.5	154.3	299.9

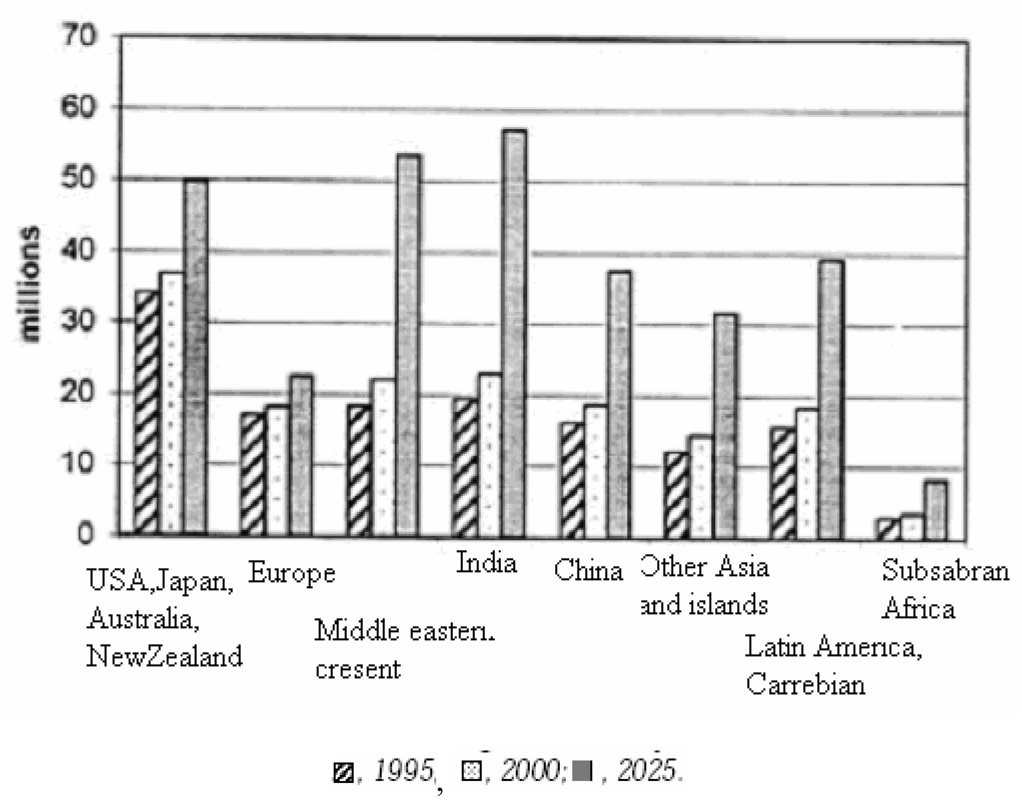

Fig 1.2 Number of people with diabetes in the adult population (>20 Years) by year and region [31]

1.3 Thesis Objective

Biamorph actuators (displacement of ~1 mm and blocking force of ~ 0.5 N) and stack actuators (displacement of ~1 μm and blocking force of ~ 1 kN) represent two extreme ends of current actuation technology. But there is lack of simple piezoelectric actuator design which can provide a high force-high displacement in low frequency range of ~2 kHz from small size (~7 x 7 x 30 mm^3). These actuators if developed can find an immediate applications in micropump (~3 kHz), localized cooling in electronics and in precise fuel injection system. This thesis addresses this issue.

The objectives of this thesis are as following: (1) develop a PZT based soft piezoelectric ceramic suitable for actuator application (2) use this material to develop a small size piezoelectric actuator which can provide large displacement and blocking force in the low frequency range of ~2 kHz, and (3) use this developed actuator for fabricating a valveless micropump.

The thesis is divided in five chapters. Chapter 1 introduces the motivation behind this work. Chapter 2 discusses the basic theory of piezoelectricity. It also describes the processing technique and characterization of the piezoelectric materials. Chapter 3 illustrates the actuator design, FEM analysis and characterization of actuator (displacement and vibration velocity as a function of applied voltage). Chapter 4 elaborates the micropump operation principle, nozzle/diffuser design, and pump design. Chapter 5 covers the extension of this work to an actuator for high frequency application. In this chapter effect of various parameters such as metal cap material, metal cap thickness, ceramic dimensions, cavity depth and cavity dimensions on the performance of the actuator are discussed. Chapter 6 describes the future scope of this work.

CHAPTER 2

MATERIALS FOR PIEZOELECTRIC ACTUATOR

2.1 Piezoelectricity

The properties of piezoelectricity were first discovered by Pierre and Jacques Curie in 1880 and have been studied for over 100 years in single crystal materials such as quartz, tourmaline, and ferroelectric Rochelle salt. The first polycrystalline material to be studied in detail was barium titanate ($BaTiO_3$), which was discovered independently by a number of researchers during the1940's in the midst of World War II. [33].The next big advancement occurred with the discovery of the lead niobate system by Goodman in 1952 and the discovery of the commercially significant lead zirconate titanate (PZT) system by Jaffe, Roth, and Marzullo in 1954.

The piezoelectric effect is the ability of certain materials to produce an electric charge proportional to an applied mechanical stress. This is known as the direct piezoelectric effect. The electric charge can also be produced in the reverse direction, by reversing the direction of applied stress. The piezoelectric effect is reversible which implies that when an electric field is applied a mechanical strain is created in the material. The piezoelectric effect is defined as a linear relationship between a mechanical variable (strain S or stress T), and an electric variable (electric field E or electric displacement D).

$$P_i = d_{ijk} T_{jk} \qquad 2.1$$

where d_{ijk} is the piezoelectric charge constant or piezoelectric strain coefficient. The converse piezoelectric effect is mathematically expressed by:

$$S_{ij} = d_{kij} E_k \qquad 2.2$$

where S_{ij} is the strain developed in the material when the electric field E_k is applied. For a given material, the piezoelectric constant d_{kij} is numerically identical for both the direct effect it the unit of Coulomb/Newton (C/N) and the converse effect in the unit of meter/Voltage (m/V).

A necessary condition for the occurrence of piezoelectricity is the absence of a center of symmetry in the crystal structure [34]. The piezoelectric behavior can be understood by considering an example of a single unit of a tetragonal perovskite ABO_3 structure as shown in Figure 2.1. This is a common piezoelectric structure. Each unit consists of a small tetravalent metal Ti, Zr in a lattice of large divalent metal ions, Pb or Ba and O ions. Under certain temperature, called Curie temperature (T_c) the structure has tetragonal, orthorhombic or rhombohedral symmetry and shows a net dipole moment. Above T_c it has simple cubic crystal structure with no dipole moment.

2.2 Ferroelectricity

Ferroelectricity was discovered in 1921 by Valasek. Ferroelectric materials are subgroups of piezoelectric materials. On application of external electric field, the ferroelectric materials have the ability to reverse the direction of spontaneous polarization. To allow the dipole to change direction, the “energy hump” between the

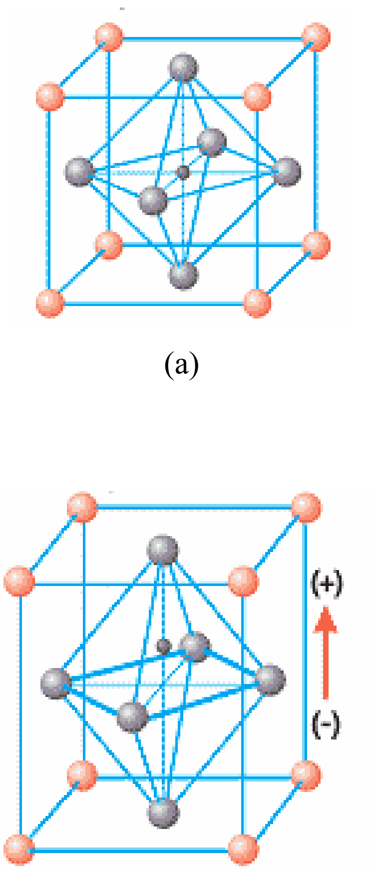

(a)

(b)

● A^{2+}= Pb, Ba other divalent metal ion

● O^{2-}= Oxygen

• B^{4+}= Ti, Zr other smaller tetravalent metal ion

Fig 2.1 Perovskite crystal structure, (a) $T>T_c$: Cubic lattice, symmetric arrangement of positive and negative charges, (b) $T<T_c$: Tetragonal (orthorhombic) lattice, crystal has electric dipole [23]

two bidirectional states must be fairly low. This implies that there exist the nonpolar state which is slightly unstable and raising the temperature will cause the transformation to the nonpolar form [33]. These materials are characterized by the presence of the remanence polarization which corresponds to the magnitude of charge stored in the material under zero applied electric field.

2.2.1 Curie temperature and phase transitions in ferroelectrics

Ferroelectrics undergo a phase transition corresponding to change in the crystal structure at particular temperature. The Curie temperature T_c represents the transition from ferroelectric to paraelectric phase. At the Curie temperature the dielectric constant reaches its maximum value. Above the Curie temperature, the crystal is paraelectric and does not exhibit any ferroelectricity and the dielectric constant follows the Curie law,

$$\varepsilon_r = C / T\text{-}T_o = \varepsilon / \varepsilon_o \qquad 2.3$$

where C is the Curie constant, T is the absolute temperature (K), T_o is the Curie-Weiss temperature (K) and ε_o is the permittivity of free space. The crystal exhibits ferroelectricity below the T_c. The ferroelectric structure is created by a distortion of the paraelectric structure. As a result the ferroelectric phase will always have a lower symmetry than a paraelectric one. The transition from the ferroelectric to paraelectric phase and corresponding changes in crystal structure and properties are shown in Fig 2.2.

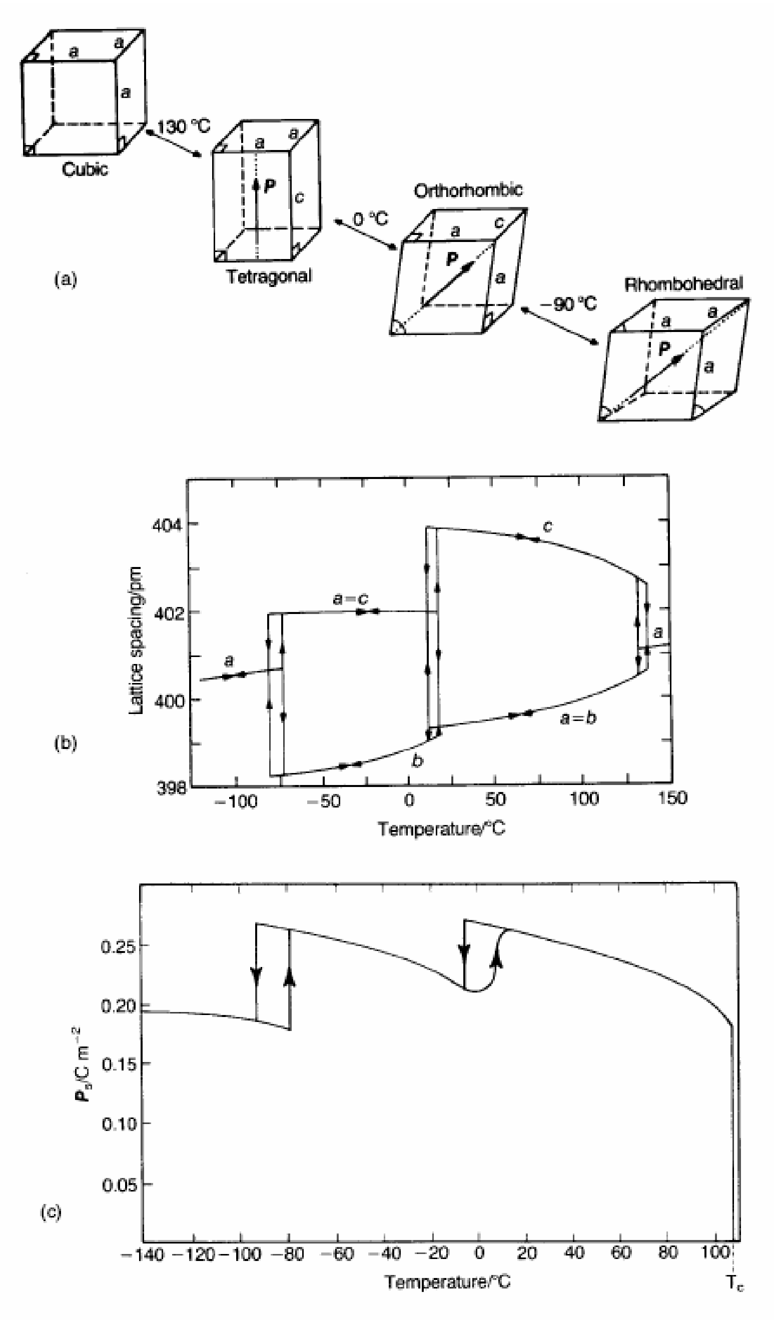

Fig 2.2 Phase transition and related changes in properties for $BaTiO_3$ with temperature (a) crystal structure, (b) lattice spacing, (c) spontaneous polarization [35]

2.2.2 Polarization process in ferroelectrics

On the application of an external electric field to a ferroelectric specimen the domains closely align to the external field direction, the process known as poling. In a ferroelectric crystal, the variety of both domain patterns and domain wall types depends on the number of possible equivalent polarization orientations. Figure 2.3 illustrates the poling process in ferroelectric specimen when an electric field is applied. The permanent dipole moment begins to rotate towards the direction of the applied electric field. On the removal of external field some of the dipole moments rotate back but not completely resulting in remanent polarization. The degree of remanent polarization is time and temperature dependent. In order to get maximum alignment the electric field is applied while the ceramic is cooling through the Curie point because at this point the dipoles are most easily aligned as they appear spontaneously. In an ideal tetragonal ceramic such as $BaTiO_3$, $1/6^{th}$ of all the domains are favorably oriented to a given field, $1/6^{th}$ switch by 180^o orientation and other $2/3^{rd}$ switch by 90^o domain orientation. The theoretical maximum polarization for a completely poled ceramic can reach 83% of the single crystal value. A bias field changes the temperature of transition and allowing the material to be used much closer to the Curie point without depoling provided that bias field has the same orientation as the original poling field. Electrical bias also increases the piezoelectric constants due to increased alignment [23, 33, 35].

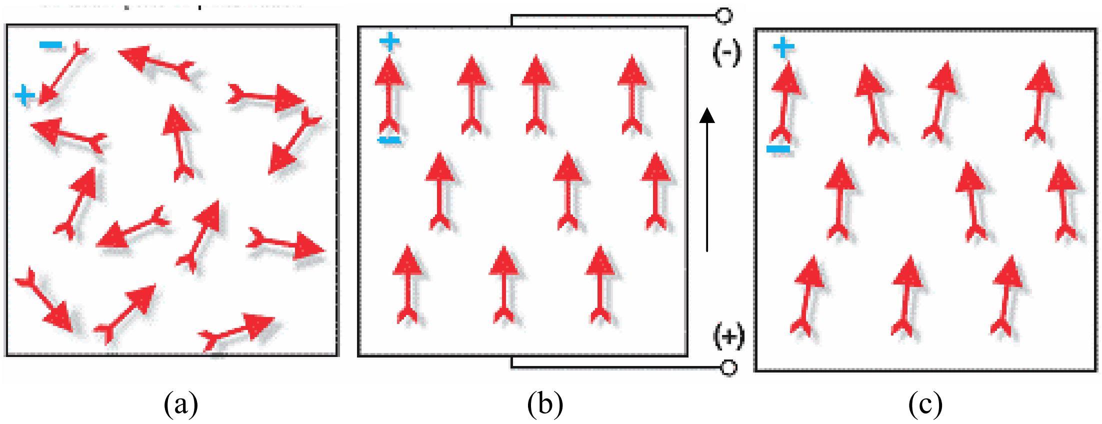

(a) (b) (c)

Fig 2.3 Polarization process in ferroelectrics, (a) Random orientation of polar domains prior to polarization, (b) Polarization process by applying DC electric field, (c) Remenant polarization after electric field is removed [23]

2.2.3 Hysteresis loop of a ferroelectric material

The hysteresis loop of the ferroelectric is as shown in the Fig. 2.4. Here polarization P is a double valued function of the externally applied electric field E. The relationship between P and E remains linear when a small electric field is applied. This is because the domains stay in their initial configuration. As the applied electric field increases, the domains with polarization in opposite direction to the field will be switched. Consequently, the polarization increases significantly with increasing E until all of the domains are aligned in the field direction. This state is called the state of saturation. The value of spontaneous polarization P_s is the extrapolation from the hysteresis loop at saturation point back to the polarization axis. Theoretically, this state of polarization saturation should correspond to single domain state of the crystal. When the field is decreased to zero the polarization does not return back to zero. Rather the domains remain aligned and the crystals exhibit a remnant polarization, P_r. The strength of the electric field necessary to reduce the polarization to zero is called the coercive field E_c. Further increase of the field in the opposite direction by reversing the field will produce the reverse loop. The coercive field strongly depends on the crystal perfection, time of application of field [33, 37].

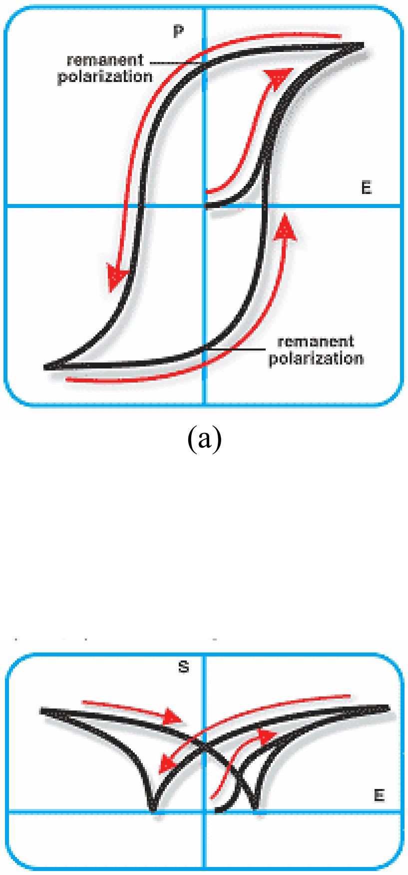

(a)

(b)

Fig 2.4 Hysteresis loop in ferroelectric materials, (a) Hysteresis curve for piezoelectric material, (b) Relative increase/decrease in dimensions (strain) in the direction of polarization [23]

2.3 The $Pb(Zr,Ti)O_3$ Crystalline Solution

Both $PbTiO_3$ and $PbZrO_3$ are perovskite type crystals. Below their respective Curie temperatures, $PbTiO_3$ is in a tetragonal ferroelectric phase, where the dipole moment in neighboring unit cells are aligned parallel; whereas $PbZrO_3$ is in orthorhombic antiferroelectric phase, where the dipole moments in neighboring cells are aligned antiparallel. The Ti^{4+} ions in $PbTiO_3$ can be partially substituted by Zr^{4+} with a molar ratio X to form binary system with following chemical formula $Pb(Zr_xTi_{1-x})O_3$. This solid solution is called lead zirconate titanate (PZT). In this solution, Zr^{4+} and Ti^{4+} occupancy on the B-site cation position is random [35].

In Fig 2.5 T_c is the temperature corresponding to the separation of the cubic paraelectric phase from various possible ferroelectric/antiferroelectric phases. A morphotrophic phase boundary (MPB) divides the ferroelectric region in two parts, which are rhombohedral (Zr-rich side) and the tetragonal (Ti-rich side). The MPB is located near x=52%. The width of the MPB depends on processing, and may also be modified by substituents. Recently, an induced monoclinic phase has been discovered around this MPB [35].

The compositions close to the MPB are of commercial interest. This is because the dielectric and piezoelectric properties exhibit maxima at these compositions. Very simplified reson for this fact is as following: in the tetragonal phase, there are six equivalent (100) polarization directions; whereas in the rhombohedral phase, there are eight equivalent (111) variants. Within the MPB region, the 6 domain states of the tetragonal coexist with the 8 domain states of rhombohedral.

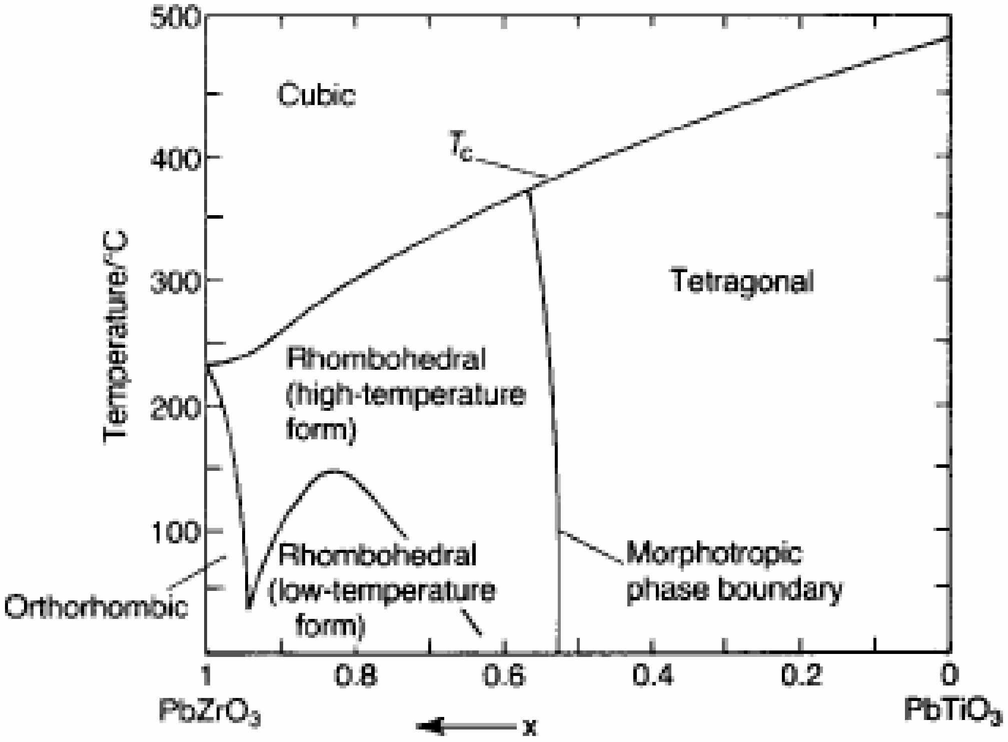

Fig 2.5 Phase diagram of PZT system near MPB [35]

This results in 14 possible directions for the spontaneous polarization. Consequently, the piezoelectric coefficient, dielectric permittivity and remanent polarization of PZT ceramics reach a maximum for compositions close to the MPB region.

2.3.1 Modified PZT ceramics

PZT ceramics are normally modified by adding substituents, which optimizes their utility for particular applications. Substituents are known to result in significant changes in domain structures and electromechanical properties, because they create various types of defects in the crystal structure. Defect may result in (i) an increased coercive field E_c if they are randomly distributed, or (ii) an internal biasing of the hysteresis loop, if the defect dipoles have the same orientation. There are three general types of substituents. These are (i) isovalent, which slightly affect properties, (ii) lower valent that tend to be charge compensated by oxygen vacancies in pervoskites, (iii) higher valent that tend to be compensated by Pb vacancies. Lower valent substituents tend to make PZT “harder”, whereas, higher valent ones make it “softer” [36].

2.3.1 (a) Soft PZT

Soft PZT behaviour is induced by addition of higher valent substituents in PZT. For example, La^{3+} or Nd^{3+} can be substituted into the A-site, whereas Nb^{5+} or Sb^{5+} on the B-site. Soft ferroelectrics have higher dielectric constants, higher dielectric and mechanical loss factors, higher elastic compliances, and higher piezoelectric coefficients. However, they have lower Curie temperatures T_c. Soft ferroelectrics also de-pole relatively easily. Amongst the soft PZT’s modified PZTs$(Pb_{1-3/2y},La_y)(Zr_{1-}$

${}_{x}Ti_{x})O_3$ crystal or PLZT is a common crystalline solution widely used in the optical applications[23, 35, 36].

2.3.1(b) Hard PZT

Hard ferroelectric characteristics can be induced by substituting lower valent ions on the A or B site. For example, the A-site position can be substituted with K^+ or Na^+; whereas Fe^{2+} or Mn^{2+} can be substituted on the B-site. Hard ferroelectrics have higher coercive field E_c, but have lower dielectric and piezoelectric constants, lower dielectric losses and lower electromechanical coupling factors. Domain boundary pinning effects are believed to be the origin of 'hard" ferroelectric behavior. Interactions between defects and domain boundaries are believed to stabilize the microstructure and make domain wall motion difficult [36].

2.3.1 (c) Relaxor ferroelectrics

Relaxor materials are modified or compound piezoelectric materials. In contrast to the conventional piezoelectric material, the phase transition doesn't occur at a specific temperature but instead occurs over a wide temperature range. A large frequency dependence of the Curie temperature T_c is observed. Relaxor ferroelectric behavior is found in compounds of type $Pb(Mg_{1/3},Nb_{2/3})O_3$. Relative insensivity to temperature and high electromechanical coupling factors exhibited by single crystals of some relaxor formulations make these materials very attractive for actuator, transducer and other application [36].

2.4 Synthesis of Piezoelectric Ceramic for Actuator in this work

The piezoelectric ceramic used for the actuator developed in this study was based on modified PZT composition around MPB, $Pb(Zr_{0.52}Ti_{0.48})O_3$. The high piezoelectric and dielectric constant, ease of poling, higher coupling factors and lower losses are the factors considered in selecting the PZT additives. It was doped with donor ions Nb^{5+} by adding Nb_2O_5 and PbO and the synthesized composition can be represented as $Pb(Zr_{0.52}Ti_{0.48})O_3$ + 1 mol% Nb_2O_5 + 1 mol% PbO.

To prepare the piezoelectric ceramic, conventional ceramic processing was used as follows:

(i) Fine powders of component metal oxides were mixed in specific proportions and wet ball milled for 24 hrs.

(ii) The ball milled powder was calcined at optimized temperature of 750°C for 2hrs.

(iii) The calcined powder was crushed, again ball milled for 24 hrs and than dried. Dried powder was ground and sieved.

(iv) The fine powder was pressed to the desired shape using cold isostatic press (30 ksi) for 5 minutes.

(v) Green body was sintered at optimized temperature of 1050°C for 2 hrs.

The sintered bar was cut and polished to size of 7 x 7 x 3.3 mm^3. The polished sample was printed with silver paste in specific electrode pattern and fired at 850°C for 1 hr. Room temperature electrode was printed on sample to eliminate the difficulties associated with asymmetric electrode pattern. Electroded pieces were poled by applying DC voltage at 2.5 kV/mm at 90°C across the sample thickness in silicon oil. After poling the temporary room temperature electrode was removed.

The X-ray diffraction pattern of the sintered ceramic is shown in Fig 2.6 exhibiting the perovskite crystal structure. The lattice parameters values determined from this XRD were found to be as: a = b = 4.036 Å (100) and c=4.146 Å (001).The microstructure of the synthesized piezoceramic is shown in fig 2.7. The high magnification SEM image revealed the dense microstructure. Dielectric constant and dielectric loss were measured using the homebuilt dielectric measurement system using HP 4284A capacitance meter. The measured dielectric data is shown in Fig 2.8. The Curie temperature for the piezoelectric ceramic was found to be around 370 ^{o}C. Fig 2.9 (a) and (b) show the pyroelectric coefficient and polarization as a function of temperature measured using the pico amp meter HP 4140B. The polarization is zero at the Curie temperature.

Table 2.1 Processing route to synthesis piezoelectric ceramic

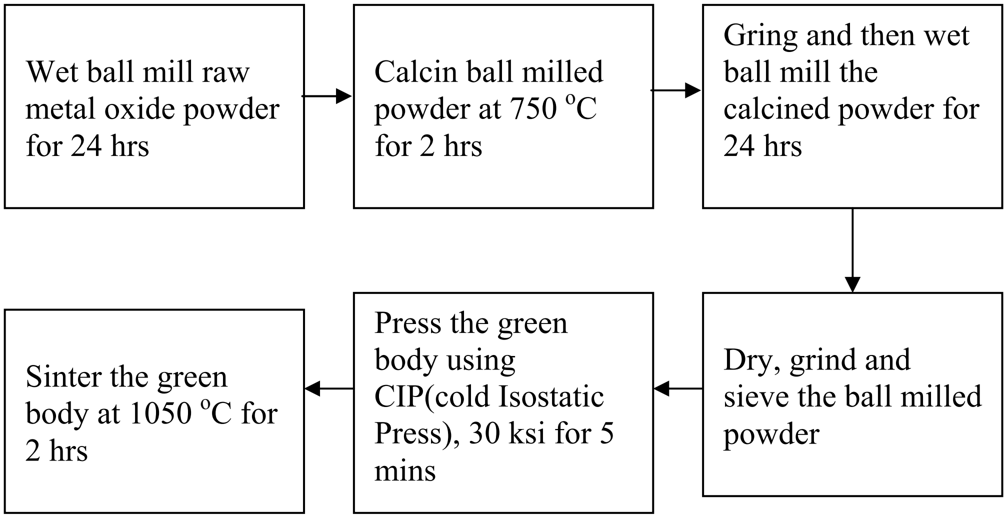

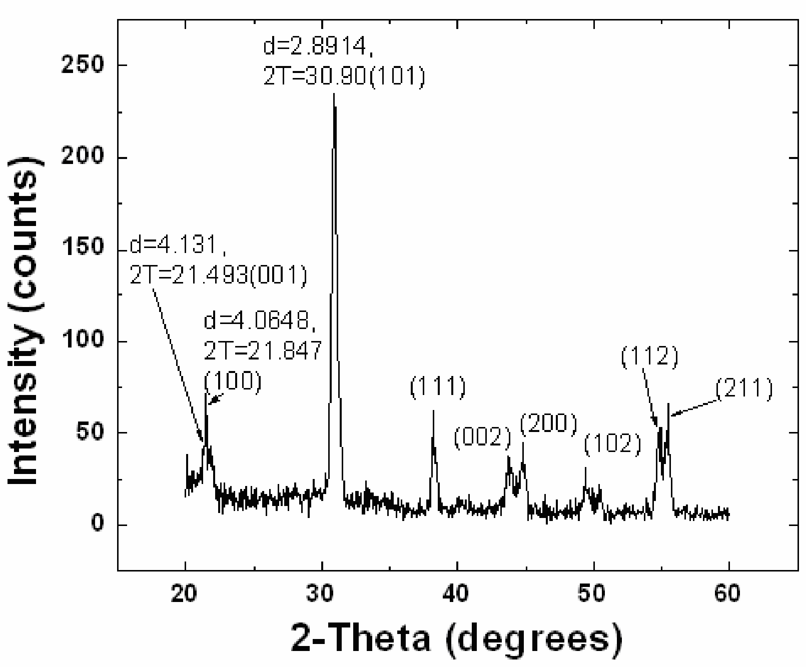

Fig 2.6 X-ray diffraction pattern of the calcined powder

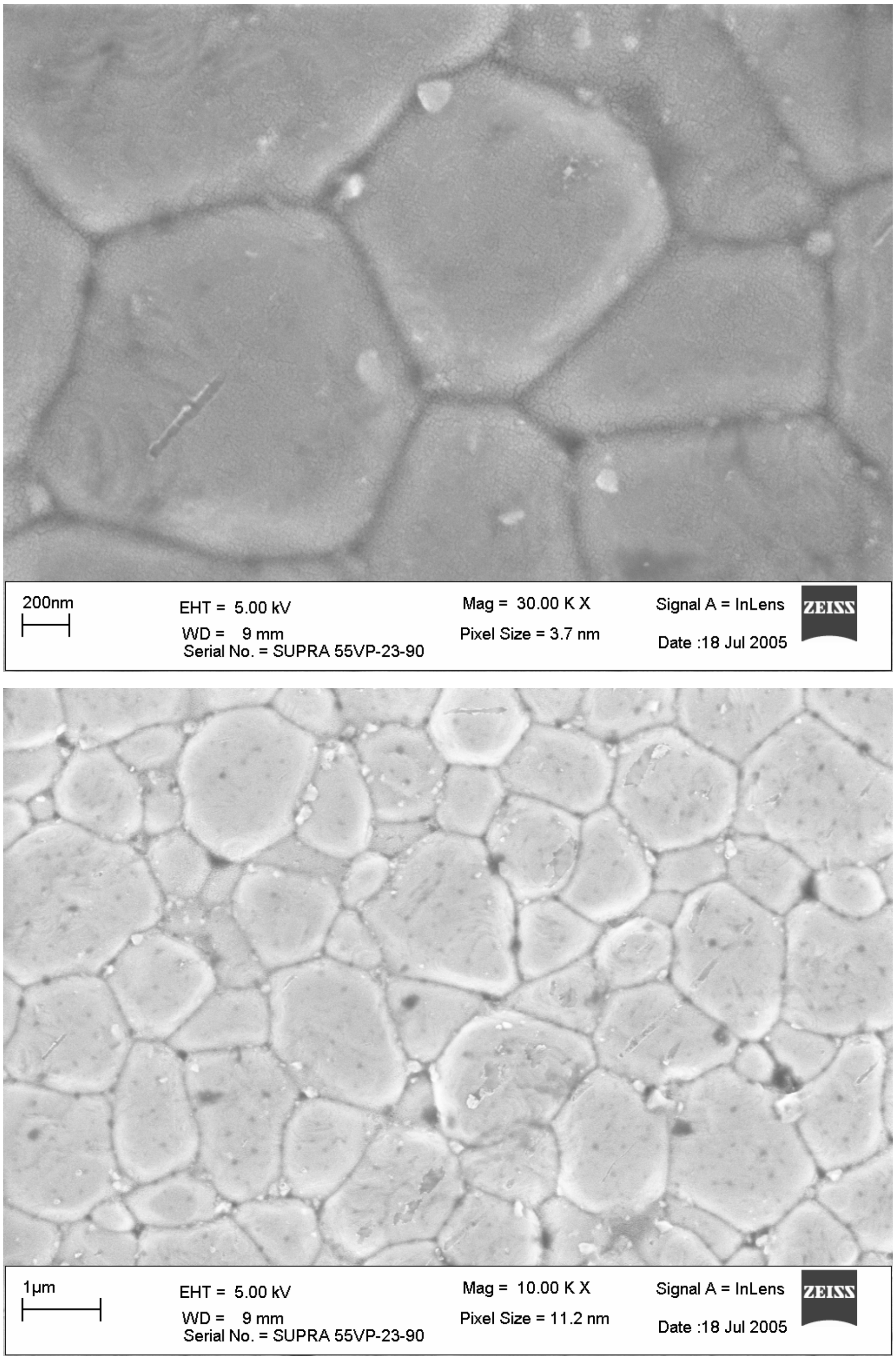

Average grain size = 1 ~ 1.5 µm

Fig 2.7 Microstructure of Piezoceramic synthesized for the actuator

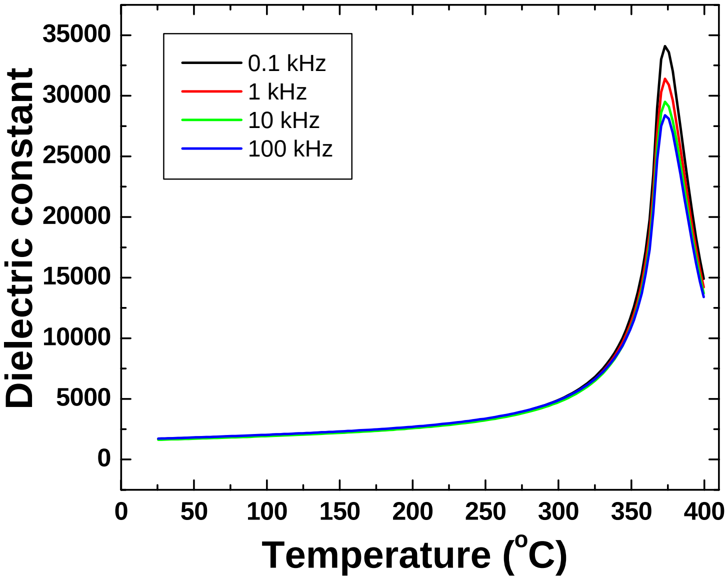

(a)

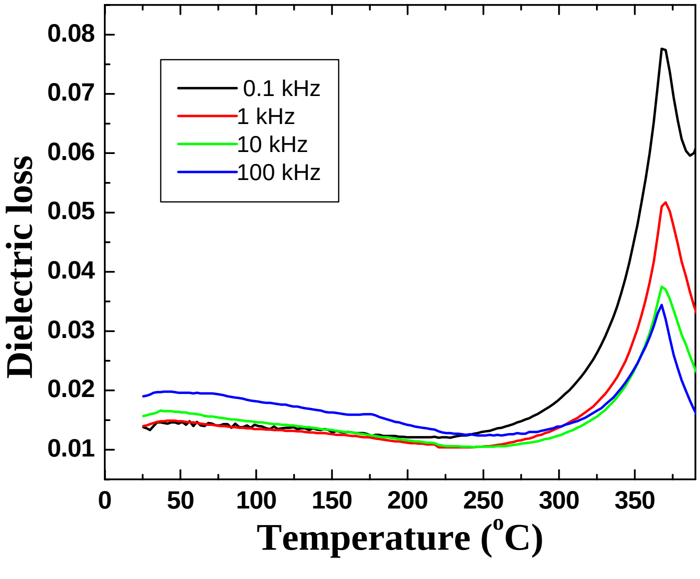

(b)

Fig 2.8 (a) Dielectric constant, (b) Dielectric loss as a function of temperature

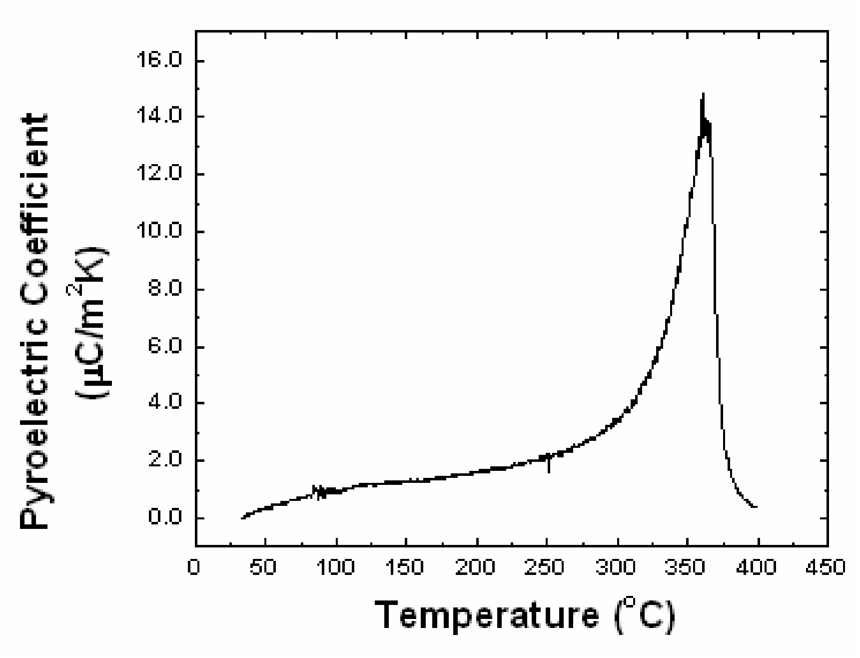

(a)

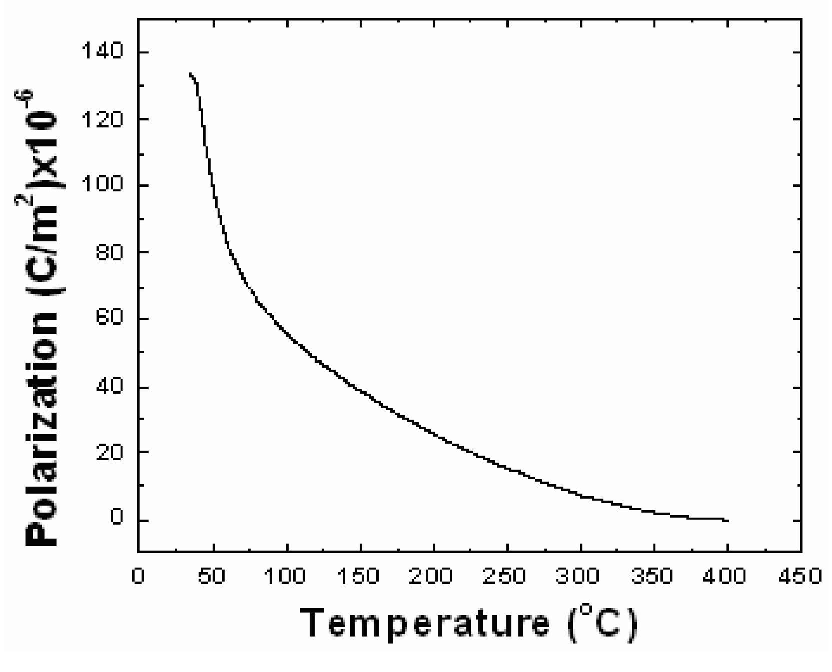

(b)

Fig 2.9 (a) Pyroelectric coefficient, (b) Polarization as a function of temperature

2.5 Parameters for Piezoelectric Devices

(a) Piezoelectric Strain Coefficient d_{ij}

The piezoelectric strain coefficient d_{ij} is important figure of merit for piezoelectric devices, especially actuator application.

It is defined by the following equations:

$$P_i = d_{ijk} T_{jk} \quad \text{and} \quad S_{ij} = d_{kij} E_k$$

A high d constant is desirable for actuator applications since the element is intended to develop motion or vibration.

(b) Piezoelectric Voltage Coefficient g_{ij}

g_{ij} is defined by following equation:

$$g_{ij} = d_{ij}/\varepsilon \qquad 2.4$$

$$\varepsilon = K\,\varepsilon_o \qquad 2.5$$

where ε and ε_o are the dielectric permittivity of the material and the vacuum, respectively. K is the dielectric constant. The g_{ij} is a figure of merit for sensor application because a material with high g is more sensitive to applied stress and can generate a high voltage.

High values of d_{33} and g_{33} are desirable in transducer design as these coefficients control the transmitting and receiving characteristic of the transducer.

(c) Electromechanical Coupling Coefficient k

This is another important parameter used to describe piezoelectric materials. The square of k is defined as the ratio of the mechanical energy stored in a piezoelectric material to the electrical energy supplied or vice versa. A high k constant means that a large portion of the input elastic energy can be transferred into electrical energy or vice versa. Since the energy conversion is always incomplete, k is always less than 1. In addition to being a material property, the magnitude of k also depends on the geometry of the device and the vibration mode and accordingly different k coefficient are defined, such as k_p(disk), k_{31}(plate-transversal vibration mode), k_{33}(bar-length extensional vibration mode), and k_t (thickness vibration mode). The $k_{effective}$ for actuator is defined:

$$k^2_{effective} = 1-(f_r/f_a)^2 \qquad 2.6$$

(d) Dielectric Constant K

It is the ratio of permittivity of the material to that of the free space. From equations 2.4 and 2.5 it can be seen that theoretically a high g_{33} constant can be obtained by decreasing dielectric constant,ε. However, if the dielectric constant is too low, several complications arise. In general, transducers made with low dielectric constant materials have small capacitance. This means that special measures must be taken in the design and construction of a transducer in order to avoid sensitivity losses due to parasitic capacitance. Transducers made with low dielectric constant materials also exhibit higher electrical impedance, and special interface electronics must be included in the system to raise the output signal (voltage) to a sufficient level for transmission. It would be useful if the performance of the materials can be optimized such that a higher d_{33} and a moderate dielectric constant, K can be obtained without degrading the sensor voltage output.

(e) Mechanical quality factor Q_m

It is defined as 2π times the maximum energy stored over one period in a small elemental volume, divided by the energy dissipated in the volume per period. Near resonance, the value of Q_m can be obtained from the impedence curve using the relation

$$Q_m = f_o/\Delta f_{3dB} \tag{2.7}$$

where f_o is the frequency corresponding to the maximum amplitude and Δf_{3dB} is the three decibel (power) bandwidth about f_o. A low Q_m material offers a wide bandwidth frequency characteristic and is therefore desirable for broadband applications. A high Q_m material offers sharp bandwidth and hence suitable for filter applications.

(f) Acoustic Impedance Z

The acoustic impedance of a propagation medium is defined in the following equation as the product of the density of the medium and the speed of sound in the medium.

$$Z = \rho\nu \tag{2.8}$$

where ρ is the density of the medium and ν is the speed of sound in the medium. The reflection and transmission of an acoustic signal at an interface between two materials are controlled by the acoustic impedance difference between the two mediums. The transmitted energy is maximized when the two impedances at the interface are matched. This requires the use of a material with impedance close to that of the load [33, 38].

Characteristics of synthesized piezoelectric ceramic

Piezoelectric properties of the synthesized ceramic were measured on a disk sample having dimension 9.87 x 1.1 mm^2. The admittance plot for the disk sample and calculated parameters are shown in Fig 2.10 and Table 2.2.

Table 2.2 Values of various parameters for the synthesized piezoelectric ceramic

Parameter	Value
Density	7.7 g/cm^3
Resonance frequency, f_r	211.25 kHz
Anti-resonance frequency, f_a	252.25 kHz
Impedance at resonance, Z_r	29.37 Ω
Dielectric constant, K	1654
Electromechanical coupling coefficient, k_p	0.619
Mechanical quality factor, Q_m	82.5
Piezoelectric charge constant, d_{33}	398 pC/N
Piezoelectric voltage constant, g_{33}	27.23 x 10^{-3} mV/N

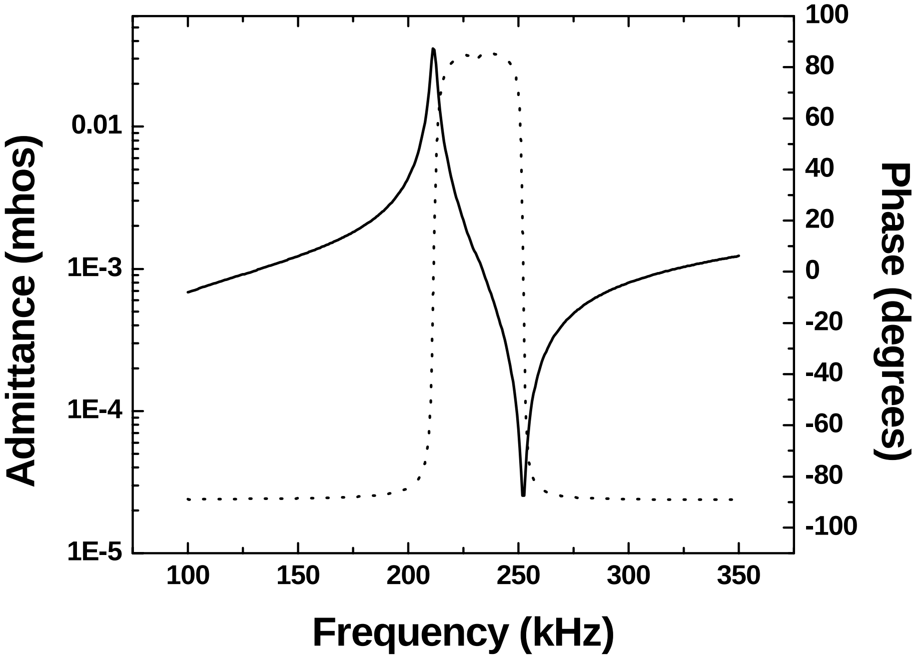

Fig 2.10 Admittance plot of the disk sample of synthesized piezoelectric ceramic

CHAPTER 3

ACTUATOR-DESIGN, FEM ANALYSIS AND FABRICATION

3.1 Actuator Design

The aim of actuator model designed in this work was to obtain the resonance frequency less than 2 kHz and simultaneously get high displacement and high force at low driving electric field of 2.5 V/mm. Fig. 3.1 shows the schematic design of the actuator.

It consists of the stack of piezoceramic pieces poled in thickness direction bonded together using epoxy (E-120HP, Loctite). The electrode pattern on each block allows the electrical connection by printing two electrode strips on the sides of stack. The stack is electrically isolated from rest of the structure by using insulation of unpoled piezoceramic on each end. The stack is then sandwiched between two steel blocks having dimension slightly larger than the ceramic pieces (0.5 mm along the height direction). Two specially designed metal caps are bonded to the steel block.

The special design of metal cap together with the steel blocks forms a mechanical amplifying mechanism for the piezostack displacement. The multilayer design of piezoceramic stacks allows the operation at low voltages. The metal caps are perpendicular to the direction of applied field it gives advantages in terms of isolating the wire connections. When voltage is applied to the piezoceramic stack the

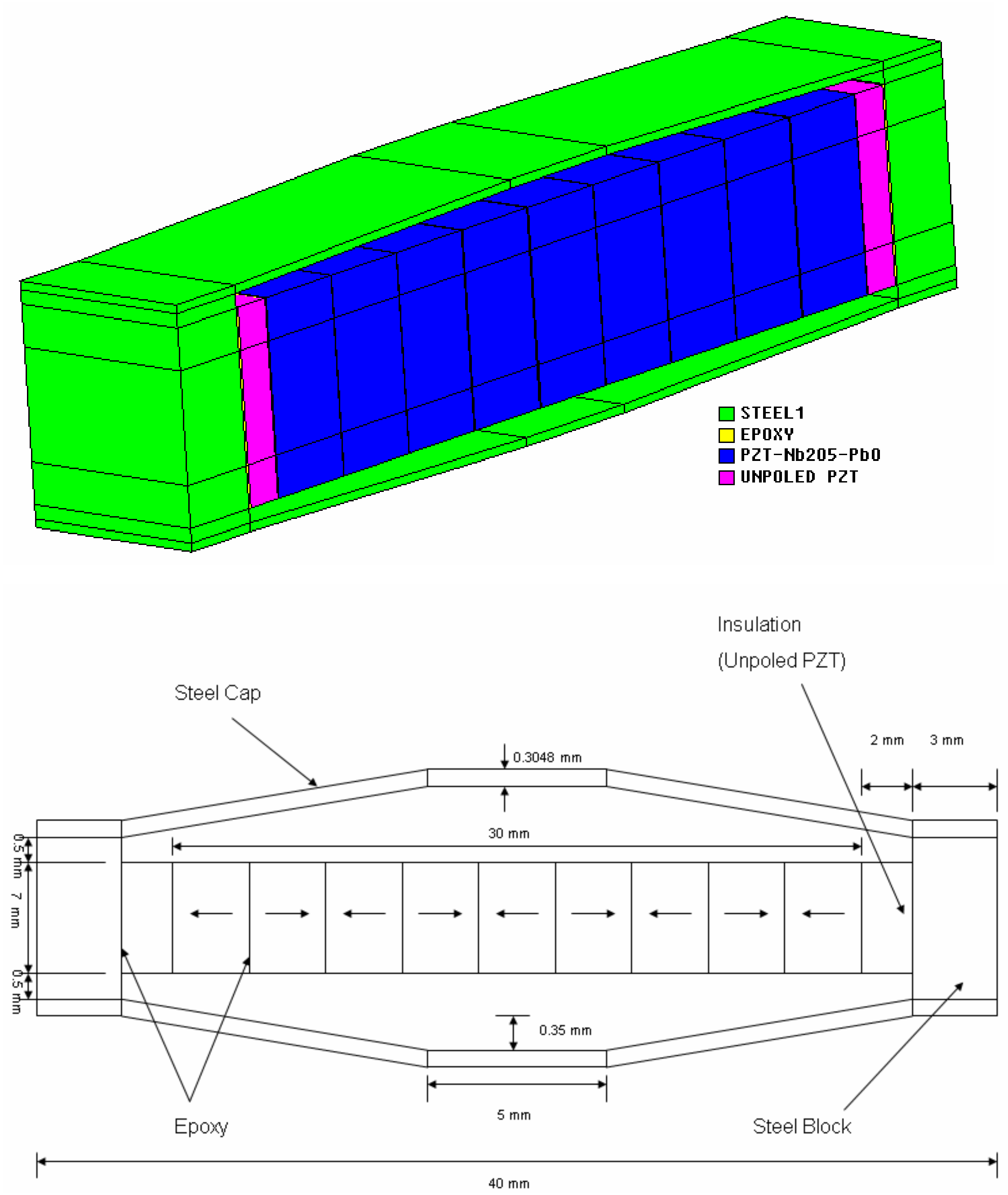

Fig 3.1 Schematic diagram of actuator design

displacement contribution from d_{33} are amplified in the transversal direction (d_{31}+Ad_{33}) where A is the amplification factor. At the same time the rigid metal cap-block structure provides prestress to the piezoceramic stack that helps the ceramic to withstand against debonding and cracking. Two different methods to rigidly attach the metal caps to steel blocks, spot welding and screws were verified and spot welding was found to be better. Fig 3.2 (a) and (b) show two actuator models made by using different techniques. Fig 3.3 (a) and (b) show the bonding layer (epoxy) thickness.

3.2 FEM Analysis of Actuator Design

The FEM Analysis of the actuator is done using ATILA GID software (Magsoft Corporation, NY). The sequence of simulation is discussed in Table 3.1.

The ATILA software allows assigning poling direction and voltage to piezoelectric material. The constitutive equations for piezoelectricity are:

$$\{T\} = \{c\}\ \{S\} - [e]\ \{E\} \qquad 3.1$$

$$\{D\} = [e]^T\ \{S\} + [\varepsilon]\ \{E\} \qquad 3.2$$

T represents 6 components of stress,

c diagonal matrix is the system stiffness matrix,

S represents 6 components of strain,

e is the piezoelectric matrix,

E represents the 3 components of the electric field,

D represents the 3 components of the electric flux density,

ε is the dielectric matrix relating the electric field to electric flux density.

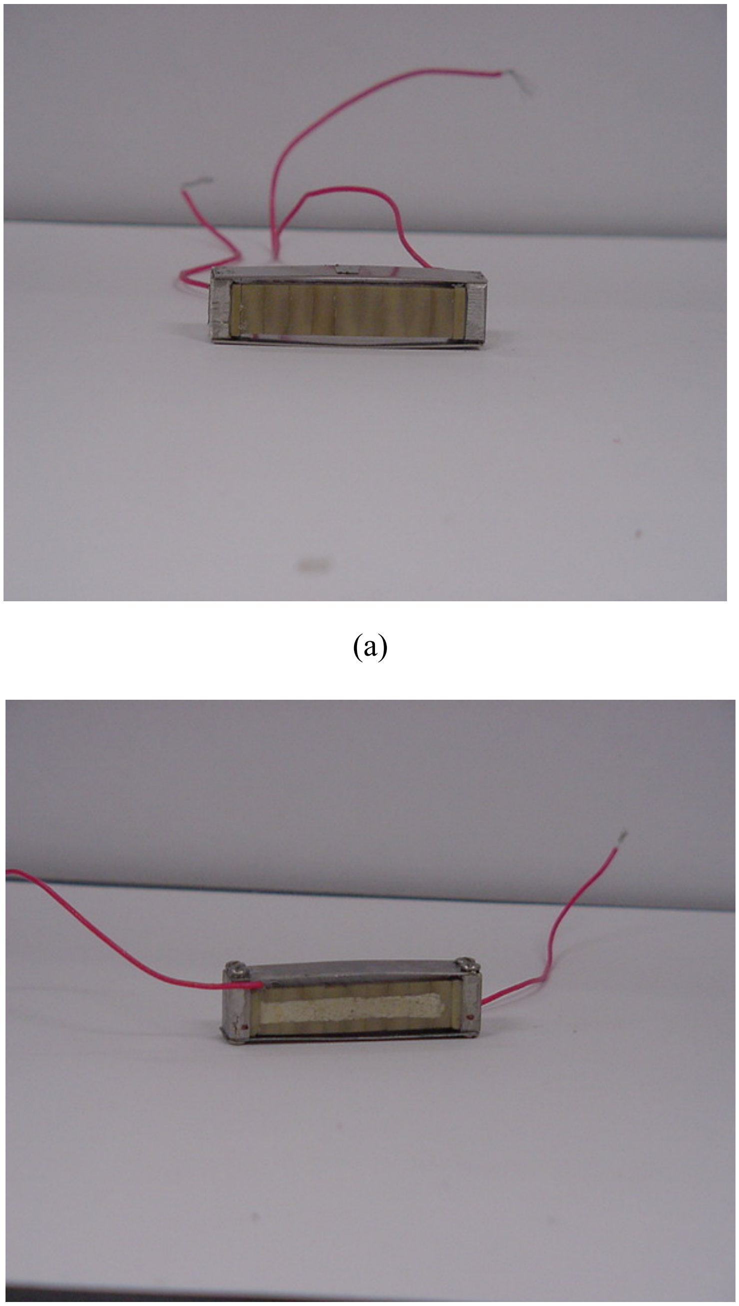

(a)

(b)

Fig 3.2 Actuator model (a) Caps are spot welded to blocks, (b) Caps are bonded to blocks using screws

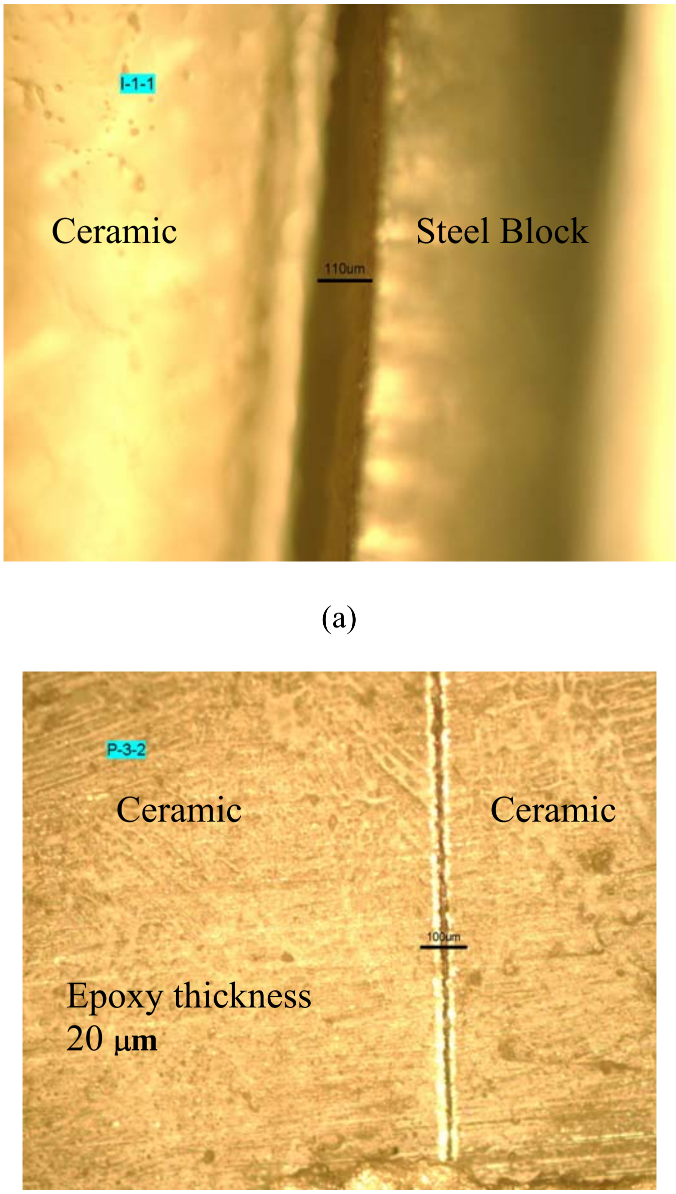

(a)

(b)

Fig 3.3 Bonding layer (epoxy) thickness between (a) ceramic-steel block (100 μm), (b) ceramic-ceramic (20 μm)

Table 3.1 Organization of simulation job in ATILA software

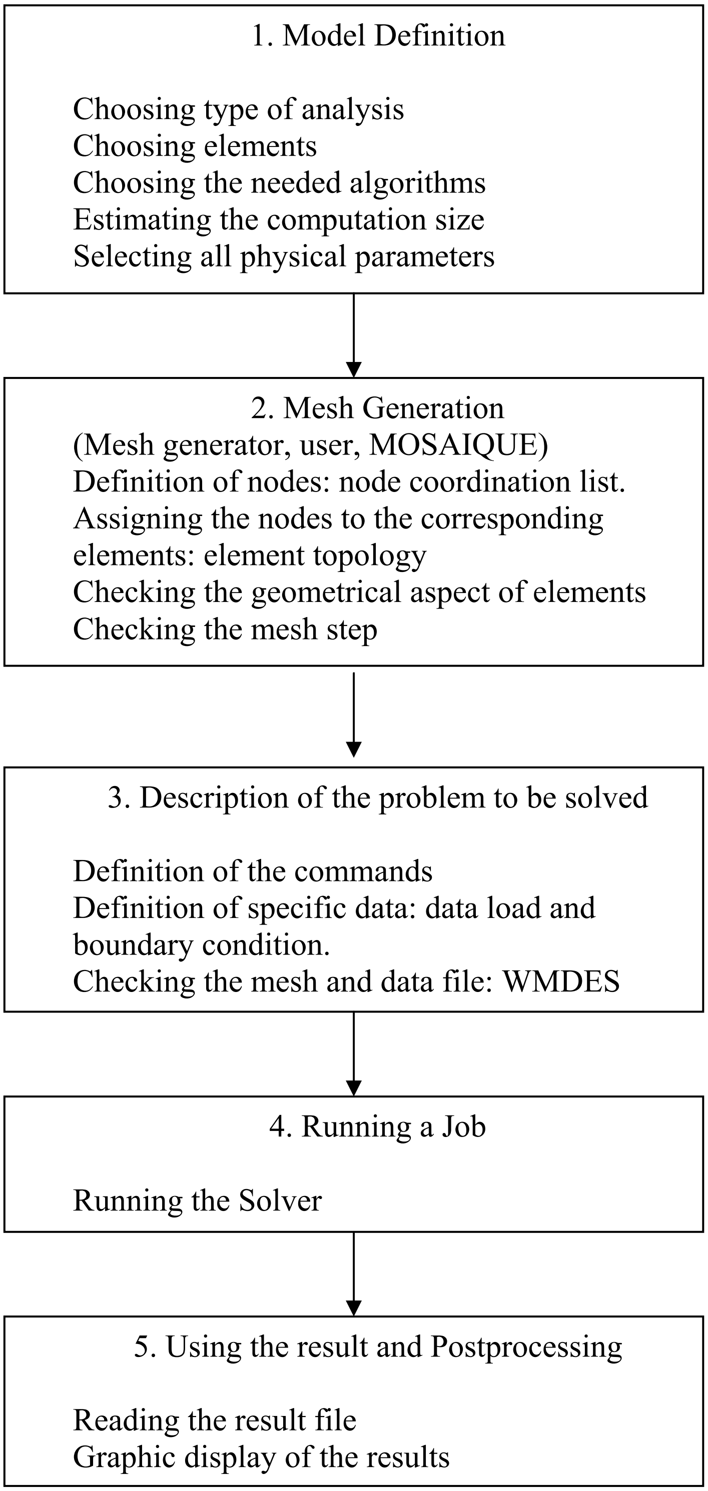

1. Model Definition

Choosing type of analysis
Choosing elements
Choosing the needed algorithms
Estimating the computation size
Selecting all physical parameters

2. Mesh Generation
(Mesh generator, user, MOSAIQUE)
Definition of nodes: node coordination list.
Assigning the nodes to the corresponding elements: element topology
Checking the geometrical aspect of elements
Checking the mesh step

3. Description of the problem to be solved

Definition of the commands
Definition of specific data: data load and boundary condition.
Checking the mesh and data file: WMDES

4. Running a Job

Running the Solver

5. Using the result and Postprocessing

Reading the result file
Graphic display of the results

The properties in equations 3.1 and 3.2 are not easily measured directly so the alternate equations are used.

$$\{S\} = [s^E]\ \{T\} + [d]\ \{E\} \qquad 3.3$$

$$\{D\} = [d]^T\ \{T\} + [\varepsilon]\ \{E\} \qquad 3.4$$

Comparing equations 3.1, 3.2 with 3.3 and 3.4 gives

$$[c] = [s^E]^{-1} \qquad 3.5$$

$$[e] = [s^E]^{-1}\ [d] \qquad 3.6$$

$$[e]^T = [d]^T[s^E]^{-1} \qquad 3.7$$

$$[\varepsilon] = [P] - [d]^T[s^E]^{-1}\ [d] \qquad 3.8$$

In above analysis, the material properties for all materials (steel, epoxy etc.) except piezoelectric material are isotropic. Equations 3.5 – 3.8 are used to generate the matrices in equations 3.1 and 3.2.

All simulations were done on 3D models. Initially, a mesh is generated using the hexahedra elements and then material properties are assigned. Table 3.2 shows the material properties of piezoelectric used for the FEM calculations. The material properties of steel are also given in Table 3.3. Once the materials are assigned in the actuator model than the next step is to assign the mechanical and electrical boundary conditions. Simulation was done at varying electric fields starting from 2.5 V/mm. Final step in the modeling of the actuator was to specify type of analysis (modal, dynamic or harmonic) and form of the output.

The admittance plot for the 7x7x40 mm^3 model (where 7 x 7 represents the area of the ceramic and 40 represents the total length of the ceramic and steel blocks, nine ceramic pieces each of thickness 3.3 mm, two steel blocks each of thickness 3 mm, and two insulation blocks each of thickness 2 mm) is shown in Fig 3.4.The resonance peak at 2.175 kHz corresponds to the flextensional mode and that at 37.6 kHz corresponds to the fundamental longitudinal mode. The flextensional mode is characterized by the displacement of cap perpendicular to the direction of the applied electric field. The longitudinal mode shows the displacement along the length of the actuator. FEM analysis was done with different sizes of ceramic 7 x 7 x 40, 8 x 8 x 40, and 10 x 10 x 40 mm^3 to find the optimum dimensions. It can be seen from Fig. 3.6 that with increasing ceramic size the resonance frequency for the flextensional mode decreases but no significant variation was found in the magnitude of the impedance. Thus, a size of 7 x 7 x 40 mm^3 was selected because lower dimensions are preferred for the pump. This actuator was than fabricated using the PZT based material described in the section 2.4.

Fig 3.5 shows the displacement at the center of the cap for the 7x7x40 mm^3 actuator model calculated using the FEM. The displacement at flextensional mode resonance frequency is much higher than that at longitudinal mode resonance frequency. This figure shows the principle of the amplification mechanism.

Table 3.2 Properties of the piezoelectric ceramic used in actuator

Properties	Magnitude	Properties	Magnitude
S_{11}^E	16.4×10^{-12}	d_{15}	584×10^{-12}
S_{12}^E	$- 5.74 \times 10^{-12}$	d_{31}	-171×10^{-12}
S_{13}^E	$- 7.22 \times 10^{-12}$	d_{33}	398×10^{-12}
S_{33}^E	18.8×10^{-12}	$\varepsilon_{11}^T/\varepsilon_o$	1730
S_{44}^E	47.5×10^{-12}	$\varepsilon_{33}^T/\varepsilon_o$	1654
$\tan\delta_m$	0.013	$\tan\delta_d$	0.02

Table 3.3 Properties of the steel used in actuator

Properties	Magnitude
Young’s Modulus	210×10^9 kg/m^2
Poisson’s ratio	0.285
Density	7.8 gm/cm^3

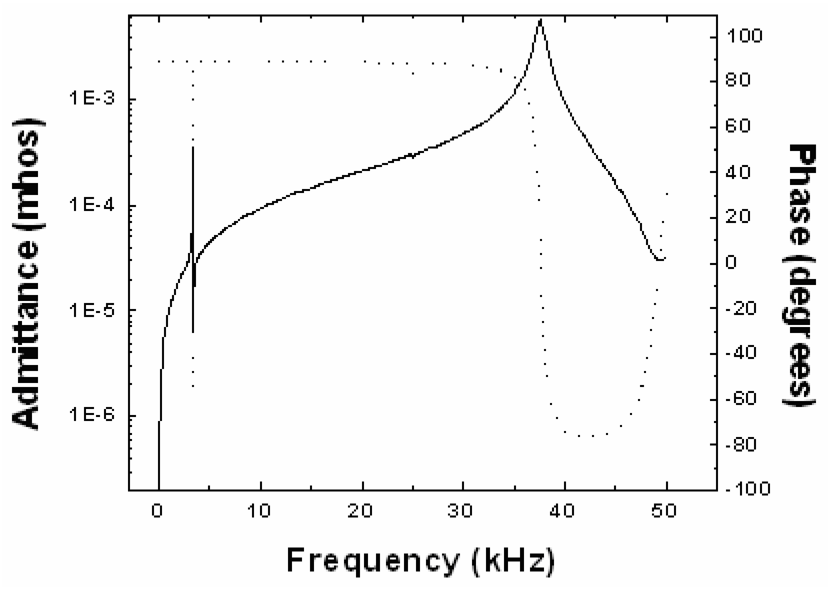

Fig 3.4 Admittance plot for the actuator model shown in Fig 3.1

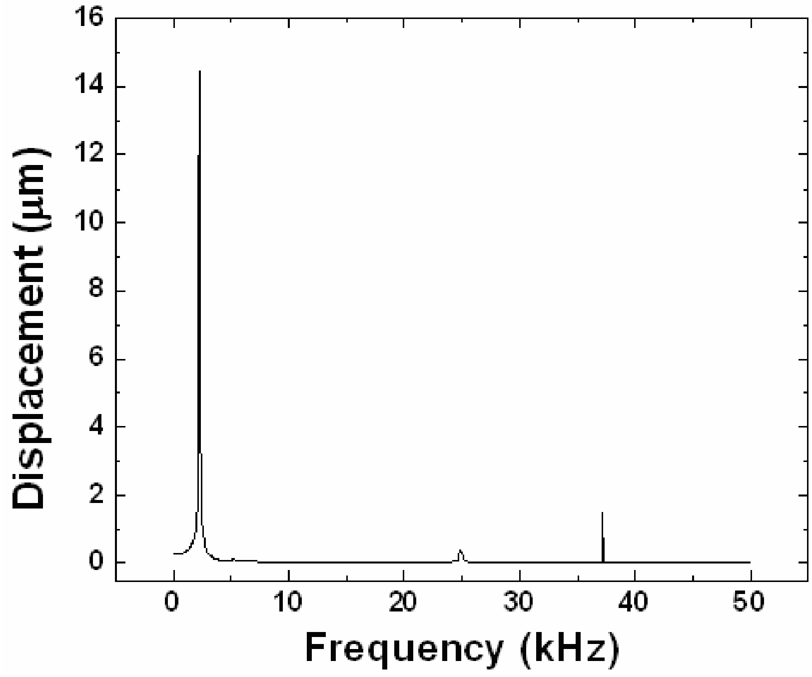

Fig 3.5 Displacement as a function of frequency for actuator design of Fig 3.1

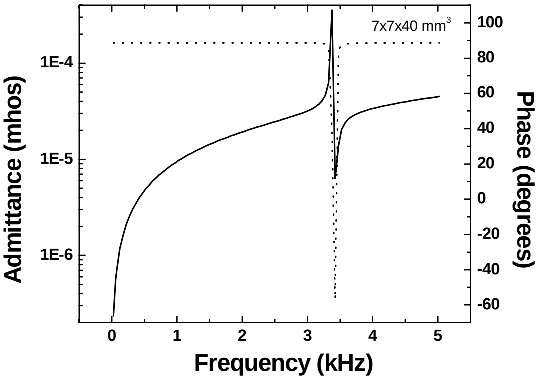

(a)

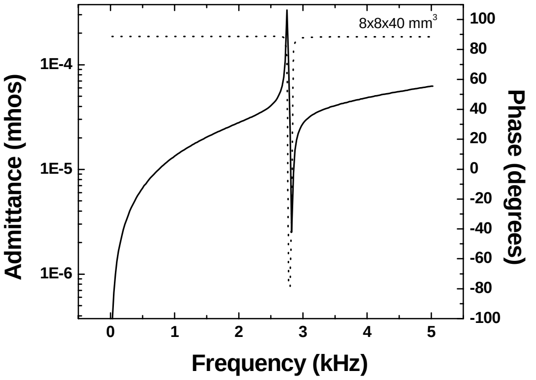

(b)

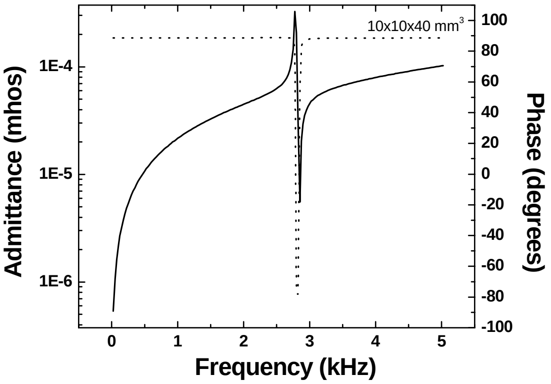

(c)

Fig 3.6 Admittance plot for different actuator sizes (a) 7x7x40 mm^3, (b) 8x8x40 mm^3, (c) 10x10x40 mm^3

In order to verify the unique design of the actuator and that the occurrence of the flextensional resonance in low frequency region is due to specially designed amplification mechanism – block + cap structure, the impedance/admittance plot were measured at each stage of actuator fabrication as shown in Fig 3.7 using HP4194 impedance analyzer. Using the admittance curve piezoelectric parameters were calculated.

It can be seen in Fig. 3.7 that no resonance peaks were observed for the single piece of ceramic of the size 7 x 7 x 3.3 mm^3 in the frequency range of 0.1 – 100 kHz. After bonding the nine ceramic pieces together only longitudinal mode resonance peak was observed for the stack at ~38 kHz. After bonding the steel blocks to the stack assembly again only longitudinal resonance peak was observed at ~28 kHz. However, after completion of the actuator design that is stack + insulation + block + metal caps both longitudinal and flextensional resonance modes were found to exist. The flextensional mode resonance peak was found to occur at 2.290 kHz. These results clearly show that the occurrence of low resonance frequency is due to special mechanical amplification mechanism.

The value of piezoelectric charge constant (d_{33}) varies with the number of pieces stacked together in actuator. Fig 3.8 shows the d_{33} values for different height of stack: single piece, stack of three pieces and stack of five pieces. Using these known values the d_{33} value corresponding to stack of nine pieces was calculated and found to be 2935 pC/N.

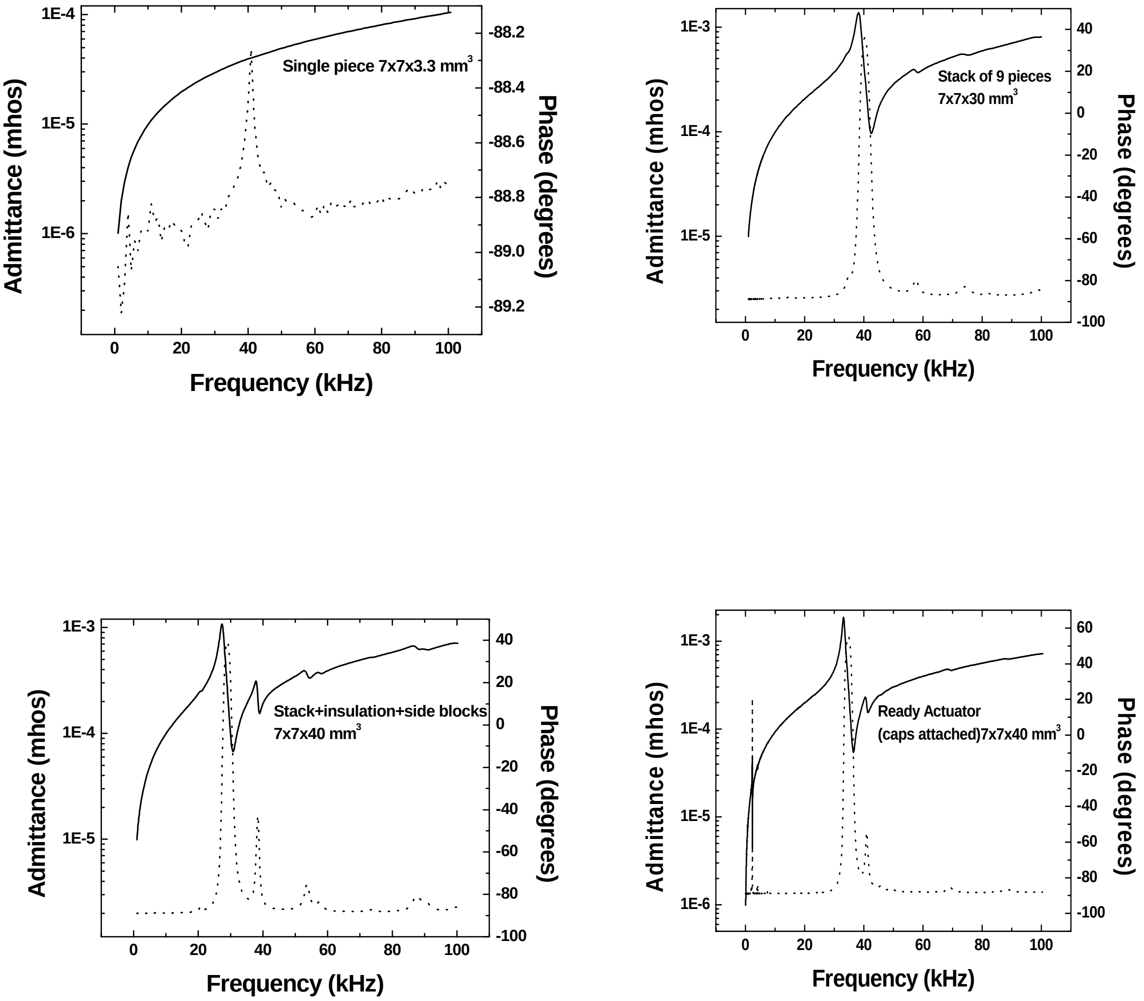

Fig 3.7 Admittance plot at different stages of actuator preparation

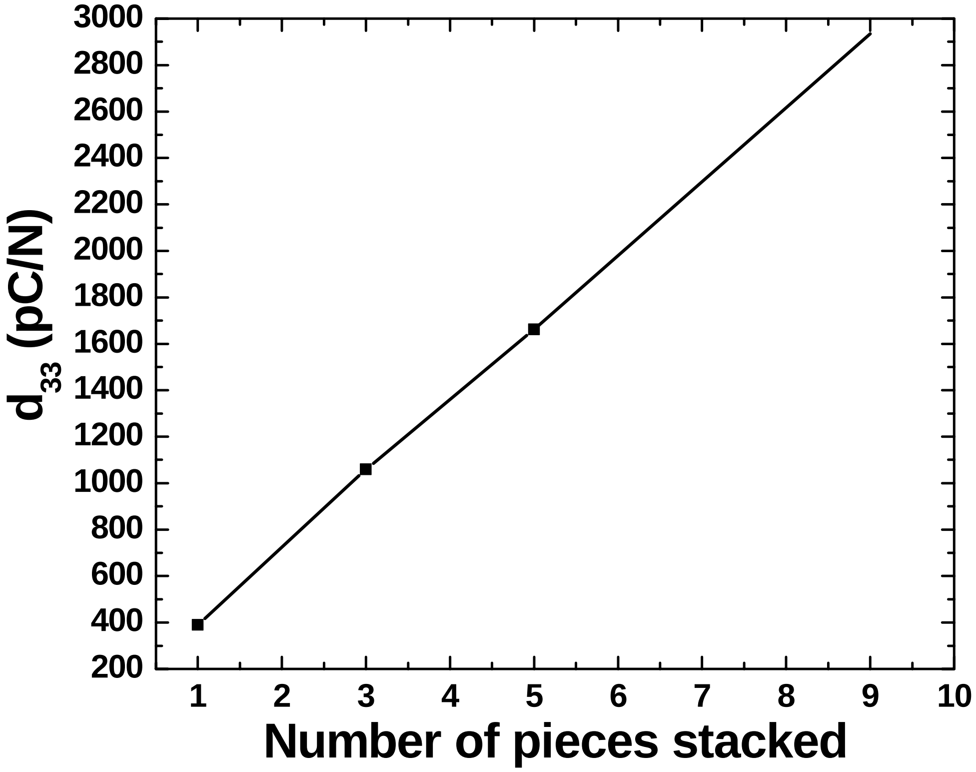

Fig 3.8 d_{33} values for different stack height

3.3 Equivalent Circuit Modeling

When the frequency of the AC electric field matches with the mechanical resonance frequency of piezoelectric element it gives maximum displacement. The behavior of piezoelectric element near to its resonance frequency is represented by the equivalent circuit, combination of L, C, R as shown in Table 3.4 and Fig 3.9.

The various symbols are:

C_o	Input capacitance
R_1	Motional resistance (Mechanical loss)
L_1	Motional inductance (Mass)
C_n	Motional capacitance (Compliance)
R_e	Series resistance
X_e	Series reactance
f_r	Resonant frequency when reactance Xe = 0
f_a	Antiresonant frequency when reactance Xe = 0
f_s	Series resonant frequency when reactance Xl = 0
f_p	Parallel resonant frequency when Re is a maximum
f_m	Frequency of maximum admittance (minimum impedance)
f_n	Frequency of minimum admittance (maximum impedance)

Table 3.4 Analogies between electrical and mechanical quantities in lumped parameter model

Mechanical Parameter	Symbol	Electrical Parameter
Force	F ↔ V	Voltage
Velocity	v = u ↔ i = q	Current
Displacement	u ↔ q	Charge
Mass	m ↔ L	Inductance
Compliance	1/k ↔ C	Capacitance
Structural Damping	c ↔ R	Resistance

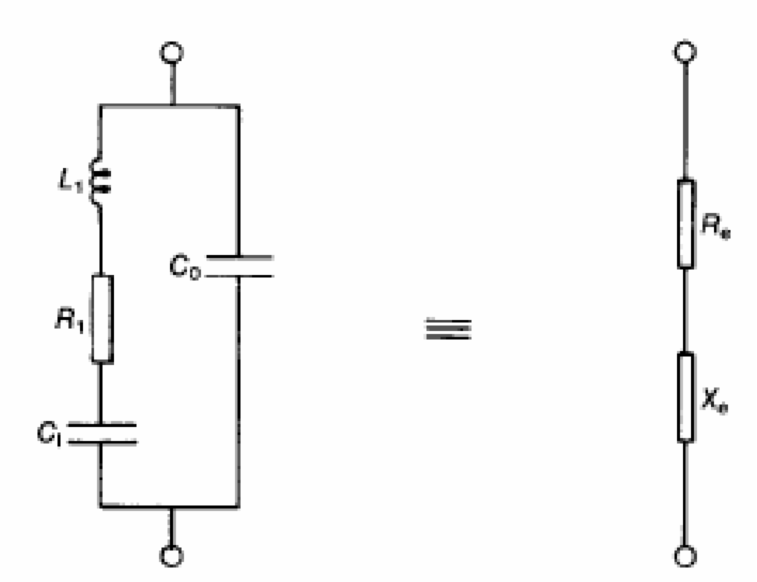

Fig 3.9 Equivalent circuit of a piezoelectric element near its resonance frequency [35]

The values of the parameters of equivalent circuit for the actuator near flextensional mode resonance frequency and longitudinal mode resonance calculated using the Impedance Analyzer (HP 4194A) are shown below.

For Flextensional mode resonance (100 ~ 5000 Hz)

R= 48.9068 kΩ , C_1=51.4963 pF

L_1=97.4830 H , C_o=1.515 nF

For Longitudinal mode resonance (100 ~ 50000 Hz)

R= 394.344 Ω , C_1=249.163 pF

L_1=86.2452 mH , C_o=1.1553 nF

3.4 Displacement measurement

The fabricated actuator was characterized for displacement and vibration velocity as a function of applied voltage. The laser Doppler vibrometer system shown in Fig 3.10 was used to measure the displacement and vibration velocity of the center node of the metal cap. Fig 3.11 shows the displacement as a function of the applied voltage. Fig 3.12(a) shows the vibration velocity for the actuator as a function of the applied voltage. The response of the actuator is almost linear during the increasing and decreasing voltage cycle as shown in Fig 3.12(b).

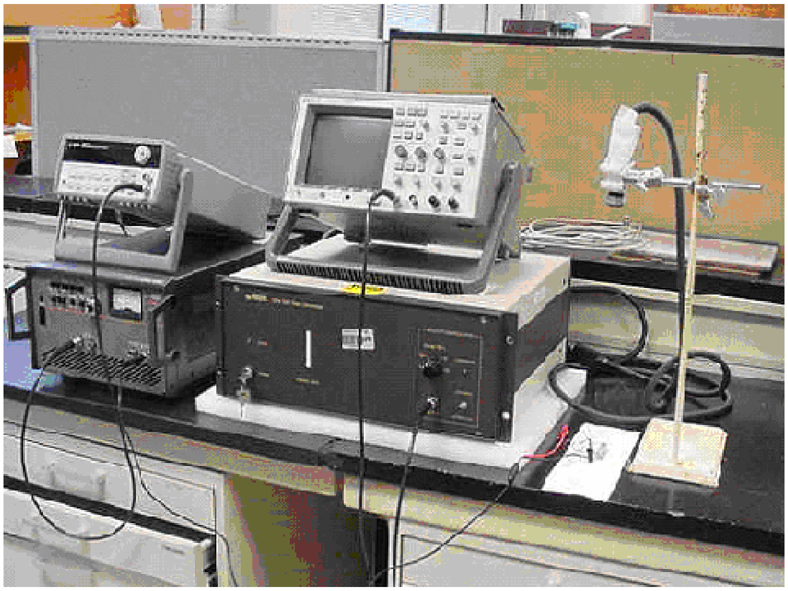

Fig 3.10 Set-up of the displacement/vibration velocity measurement system

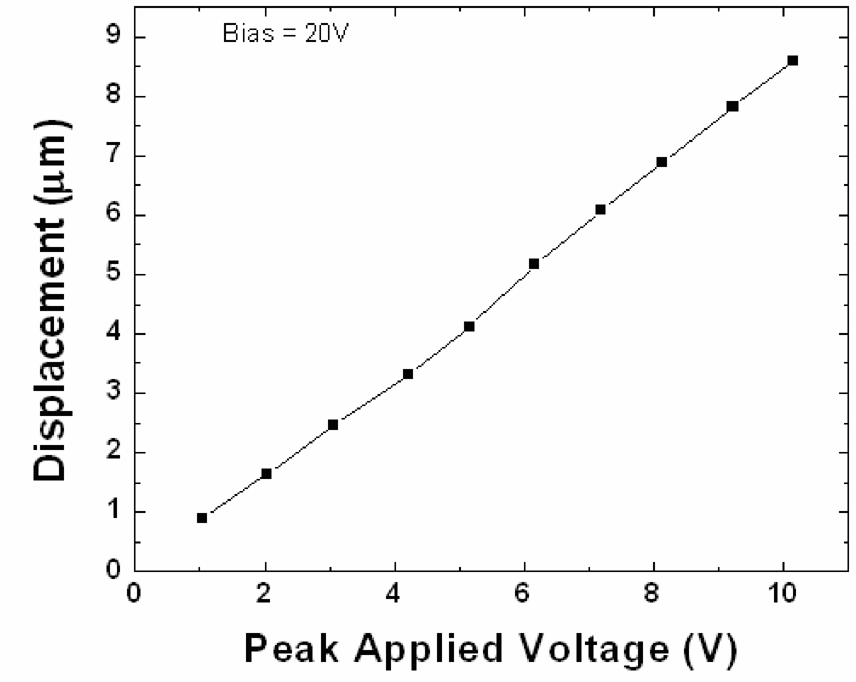

Fig 3.11 Displacement as a function of applied voltage

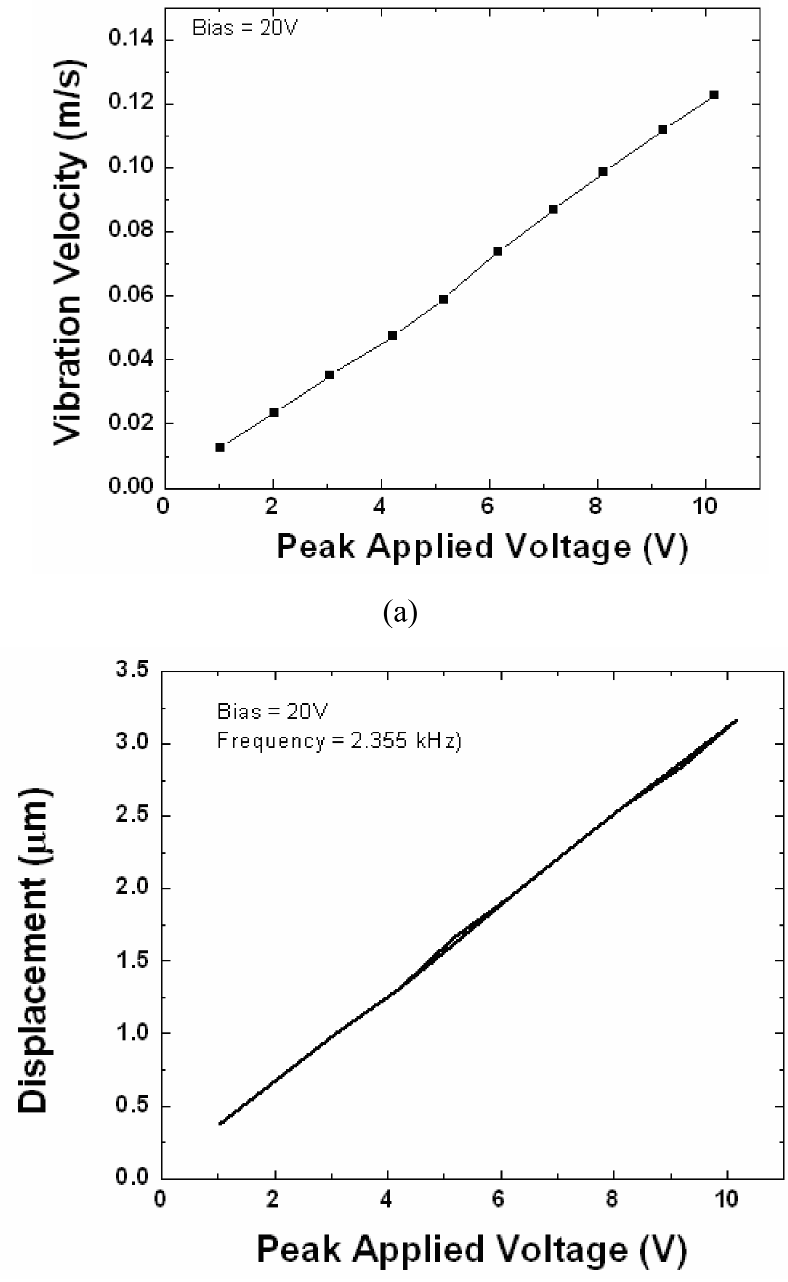

(a)

(b)

Fig 3.12 (a) Vibration velocity, (b) Displacement (hysteresis), as a function of the applied voltage

Fig 3.13(a) compares the calculated and experimental admittance plots. Fig 3.13(b) shows the comparison between the calculated and experimental displacement for the actuator. A fairly good agreement between the calculated and experimental results can be seen in this figure. The peak at ~9 kHz shows the coupling between other possible vibration modes. The difference in the results may be due to the effect of various parameters like bonding technique, alignment of pieces in the stack, electrical connection which could not be entered in the FEM model.

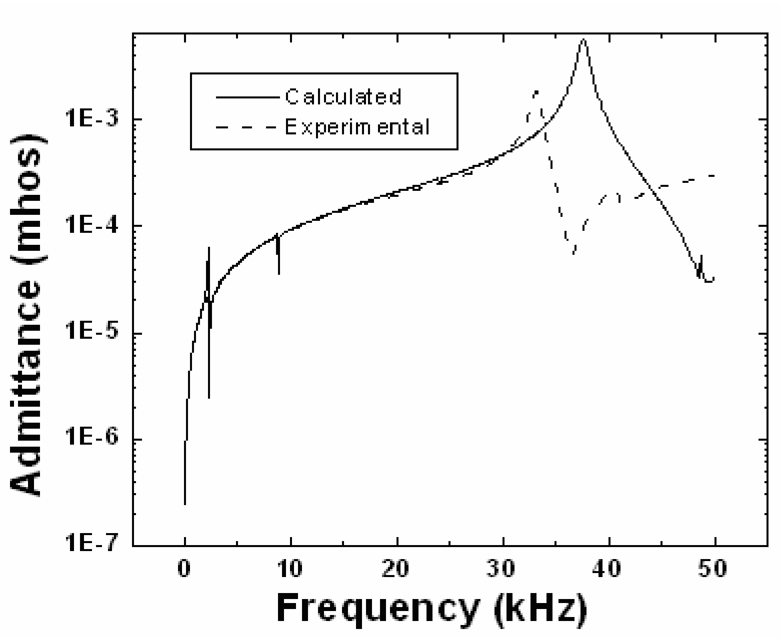

(a)

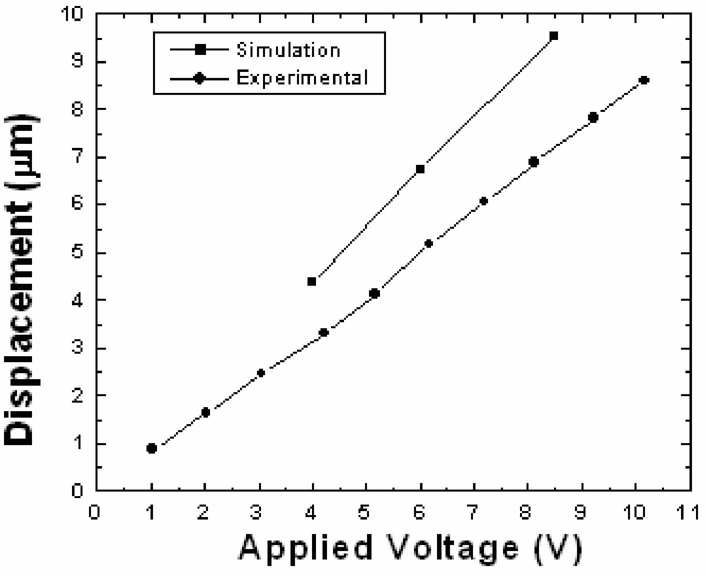

(b)

Fig 3.13 Comparison between calculated and experimental data for the actuator (a) admittance plot, (b) displacement

CHAPTER 4

PIEZOELECTRIC MICROPUMP

4.1 Introduction

Pumps are the oldest known devices used to transfer energy to fluid. In broad way pumps are classified in two category, positive displacement pump and rotary pump.

a) Positive Displacement Pump (Reciprocating Pump)

It uses the oscillatory or push-pull motion of diaphragm or piston to displace the fluid. In positive displacement pump fluid enters the pump chamber when inlet valve is open. When valve is closed the fluid is compressed by the moving surface to the outlet. Based on the moving surface the reciprocating pumps may further be divided into piston pump and diaphragm pump. A peristaltic pump is a diaphragm pump [27]. The peristaltic pumps consist of two or three pump chambers and diaphragm. Fluid is transferred from one end to the other through periodic movement of each diaphragm, excited one by one through controlled signal. Positive displacement or reciprocating pumps provides high pressure but low flow rate. They are able to pump viscous fluids also. The characteristic of positive displacement pump is that it provides pulsating or periodic flow.

b) Rotary Pump

Here energy is transferred to fluid by means of fast rotating blades or certain special designs. The momentum of fluid increases as it flows rapidly through vanes and the high velocity of fluid is converted into pressure when it exits through diffuser element. Rotary pumps provides steady, high flow rate but achievable pressure is low.

While miniaturization is revolutionizing the world of sensors and various mechanical systems, a variety of chemical and biological procedures require devices that can deliver minute and accurately metered quantity of material. This need has stimulated extensive research in the field of microfluidics in last decade. The most potential application of micropump is the controlled drug delivery, precise fuel injection system, and localized cooling of electronic devices. [39]

In this work piezoelectric actuation is used to drive the micropump. The principle of piezoelectric actuation is already discussed in chapter 1 and 3. Piezoelectric actuation is very attractive as it provides comparatively high stroke volume, and high actuation force and fast mechanical response. In addition it can be used for any fluid type. Table 4.1 compares pump operation frequency, flowrate, and pressure head for different actuation mechanisms used in pump.

Table 4.1 Different micropump principle actuation mechanisms and its performance [40]

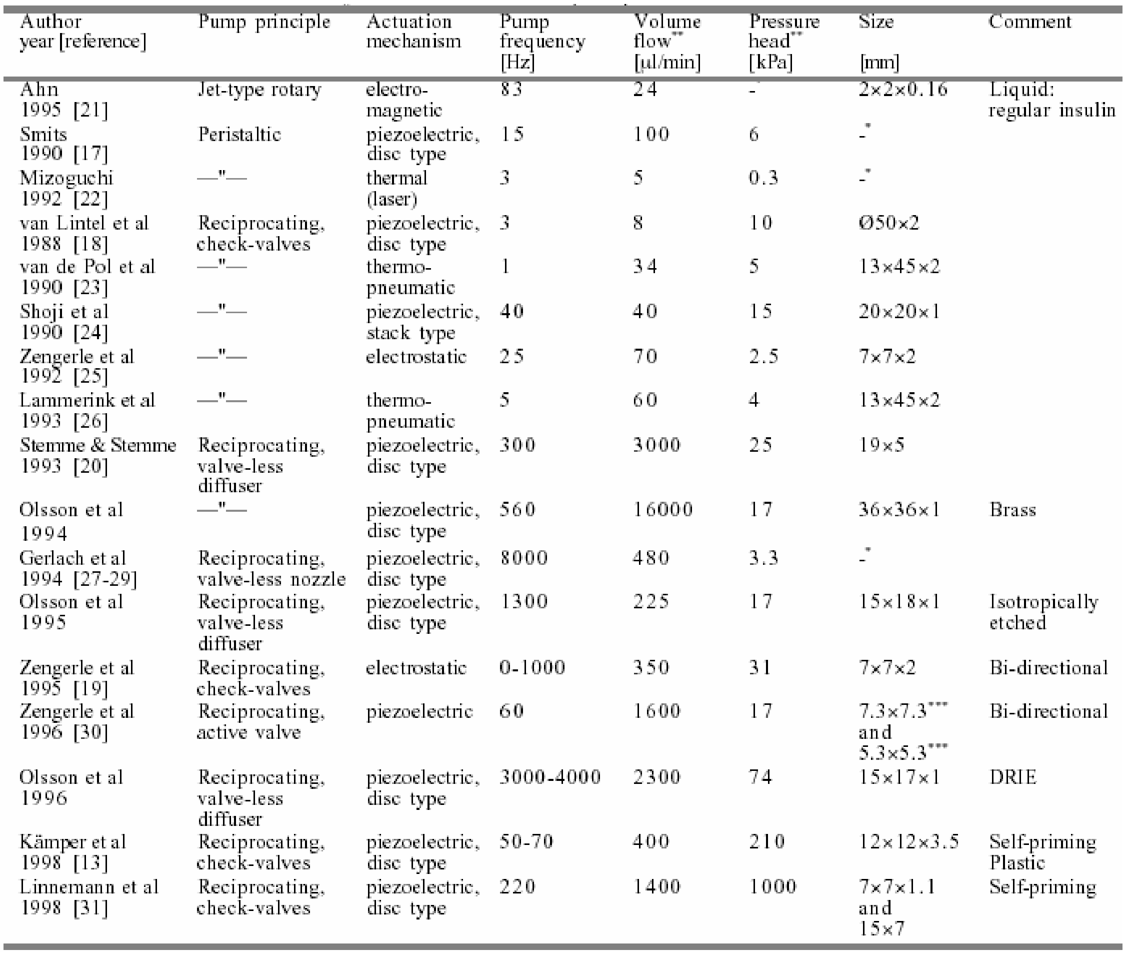

Author year [reference]	Pump principle	Actuation mechanism	Pump frequency [Hz]	Volume flow** [µl/min]	Pressure head** [kPa]	Size [mm]	Comment
Ahn 1995 [21]	Jet-type rotary	electro-magnetic	83	24	-*	2×2×0.16	Liquid: regular insulin
Smits 1990 [17]	Peristaltic	piezoelectric, disc type	15	100	6	-*	
Mizoguchi 1992 [22]	—"—	thermal (laser)	3	5	0.3	-*	
van Lintel et al 1988 [18]	Reciprocating, check-valves	piezoelectric, disc type	3	8	10	Ø50×2	
van de Pol et al 1990 [23]	—"—	thermo-pneumatic	1	34	5	13×45×2	
Shoji et al 1990 [24]	—"—	piezoelectric, stack type	40	40	15	20×20×1	
Zengerle et al 1992 [25]	—"—	electrostatic	25	70	2.5	7×7×2	
Lammerink et al 1993 [26]	—"—	thermo-pneumatic	5	60	4	13×45×2	
Stemme & Stemme 1993 [20]	Reciprocating, valve-less diffuser	piezoelectric, disc type	300	3000	25	19×5	
Olsson et al 1994	—"—	piezoelectric, disc type	560	16000	17	36×36×1	Brass
Gerlach et al 1994 [27-29]	Reciprocating, valve-less nozzle	piezoelectric, disc type	8000	480	3.3	-*	
Olsson et al 1995	Reciprocating, valve-less diffuser	piezoelectric, disc type	1300	225	17	15×18×1	Isotropically etched
Zengerle et al 1995 [19]	Reciprocating, check-valves	electrostatic	0-1000	350	31	7×7×2	Bi-directional
Zengerle et al 1996 [30]	Reciprocating, active valve	piezoelectric	60	1600	17	7.3×7.3*** and 5.3×5.3***	Bi-directional
Olsson et al 1996	Reciprocating, valve-less diffuser	piezoelectric, disc type	3000-4000	2300	74	15×17×1	DRIE
Kämper et al 1998 [13]	Reciprocating, check-valves	piezoelectric, disc type	50-70	400	210	12×12×3.5	Self-priming Plastic
Linnemann et al 1998 [31]	Reciprocating, check-valves	piezoelectric, disc type	220	1400	1000	7×7×1.1 and 15×7	Self-priming

4.2 Pump Operation Principle

The first micropump designs were based on an actuation of both the pump diaphragm and the valves [30]. But these pumps have risk of reducing pump performance and reliability due to wear and fatigue of valves. There is a high risk of valve clogging. Also the pressure drop across valves is a problem. To eliminate these problems a valve-less reciprocating pump was present for the first time in 1993 by Stemme and Stemme which overcame these drawbacks [26].

The pump presented in this work is a valve-less pump utilizing the flow directional property of nozzle/diffuser element. The diffuser is a flow channel with gradually expanding cross section, while the nozzle is a flow channel with converging cross section. Diffuser/nozzle has a property that it offers low resistance to flow in the diffuser direction than in the nozzle direction, for the same flow velocity. The pump operates in two modes: Supply and Pump modes.

1) Supply Mode

When the pump diaphragm moves up and pumps chamber volume increases the inlet element acts as a diffuser and offers lower flow resistance than the outlet element which acts as nozzle. As a result of this a larger volume is transported into the pump chamber through inlet element.

2) Pump Mode

When the pump diaphragm moves down and the pump chamber volume decreases the outlet element acts as diffuser with lower flow resistance than the inlet

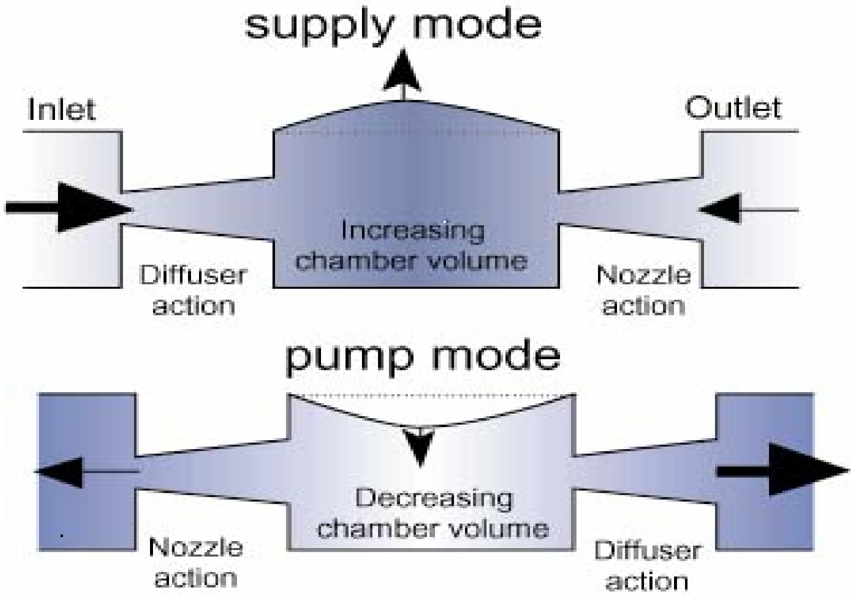

Fig 4.1 Operation principle of valveless diffuser/nozzle pump [26]

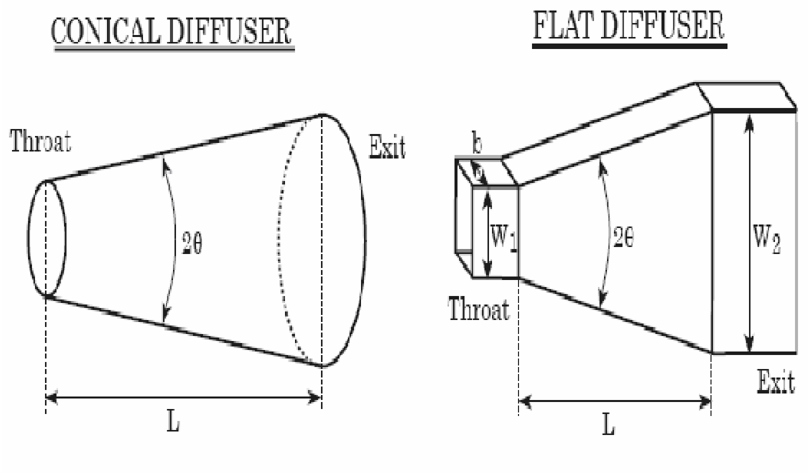

Fig 4.2 Conical and Flat wall diffusers schematic diagram [41]

element, which acts as a nozzle. As a result of this larger volume is transported out of the chamber through the outlet element.

Combined, a net volume is pumped from the inlet side to the outlet side at the end of a complete pump cycle, despite the fact that nozzle/diffuser element conveys fluid in both direction.

4.3 Diffuser/Nozzle Design

As discussed in previous section, diffuser is a duct with gradually expanding cross section and nozzle is a duct with gradually converging cross section. For the efficient operation of pump, diffuser is a key design parameter. The function of the diffuser is to transform kinetic energy, i.e. velocity, to potential energy, i.e. pressure. A 'stability map', such as shown in Fig. 4.3, can exemplify the type of flow in a diffuser. The map shows that depending on the geometry, the diffuser operates in four different regions [41].

In the *no stall* region the flow is steady viscous without separation at the diffuser walls and provides moderately good performance. In the *transitory steady stall* region the flow is unsteady. The minimum pressure loss occurs in this region. In the *bistable steady region* a stall can flip-flop from one part of the diffuser wall to another and performance is poor. In the *jet flow* region the flow separates almost completely from the diffuser walls and passes through the diffuser at nearly constant cross-sectional area making performance extremely poor [41]. Typical performance maps for diffusers are shown in Fig. 4.4. The parameter pressure recovery coefficient, C_p, defines the resultant pressure in a complete cycle, given as:

$$C_p = (p_e - p_t)/(p_{0t} - p_t) \qquad 4.1$$

where p_e is pressure at exit section, p_t is pressure at throat(inlet) section and p_{0t} is the stagnation pressure at throat section(pressure when fluid is at rest) [41].

The higher the C_P value, the better is the diffuser performance. In general, the two main types of diffusers, conical and flat-walled, have approximately the same diffuser capacity.

In Fig. 4.5 the dependence of the losses on diffuser angle is shown for diffusers with macroscopic, turbulent flow. The loss coefficient is related to the C_P value by the relation:

$$K = 1 - (A_{throat} / A_{exit})^2 - C_p \qquad 4.2$$

where A_{throat} and A_{exit} are the inlet and outlet cross sectional areas, respectively. For small angles the losses in the diffuser are small and the minimum losses occur for a cone angle 2θ equal to about 5°. For cone angles larger than 40° to 60° the loss is higher than for a sudden expansion. For these large angles, the gradual expansion does not raise the static pressure further and there is no diffuser effect. This unexpected effect is due to gross flow separation in a wide-angle diffuser. The effect is highly dependent on the inlet boundary conditions [41].

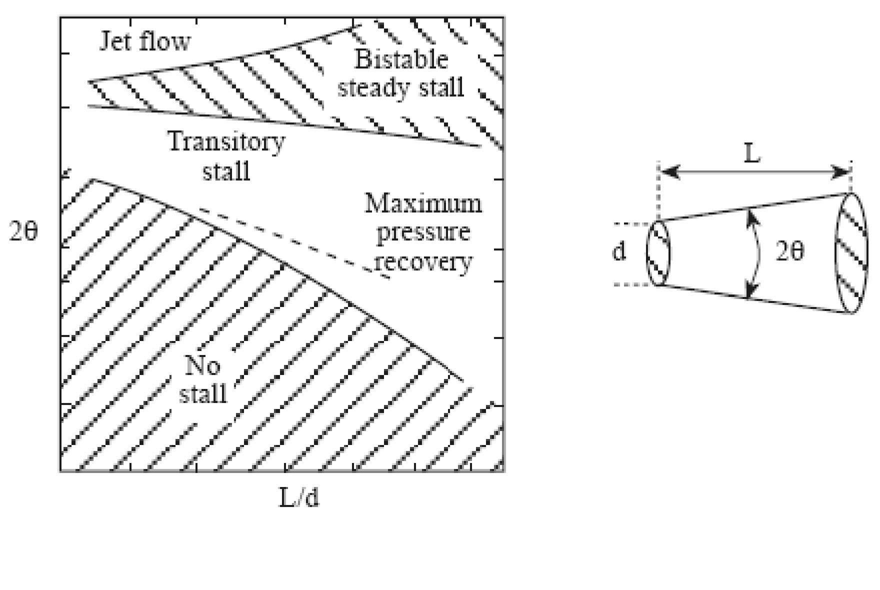

Fig 4.3 Stability map of diffuser [41]

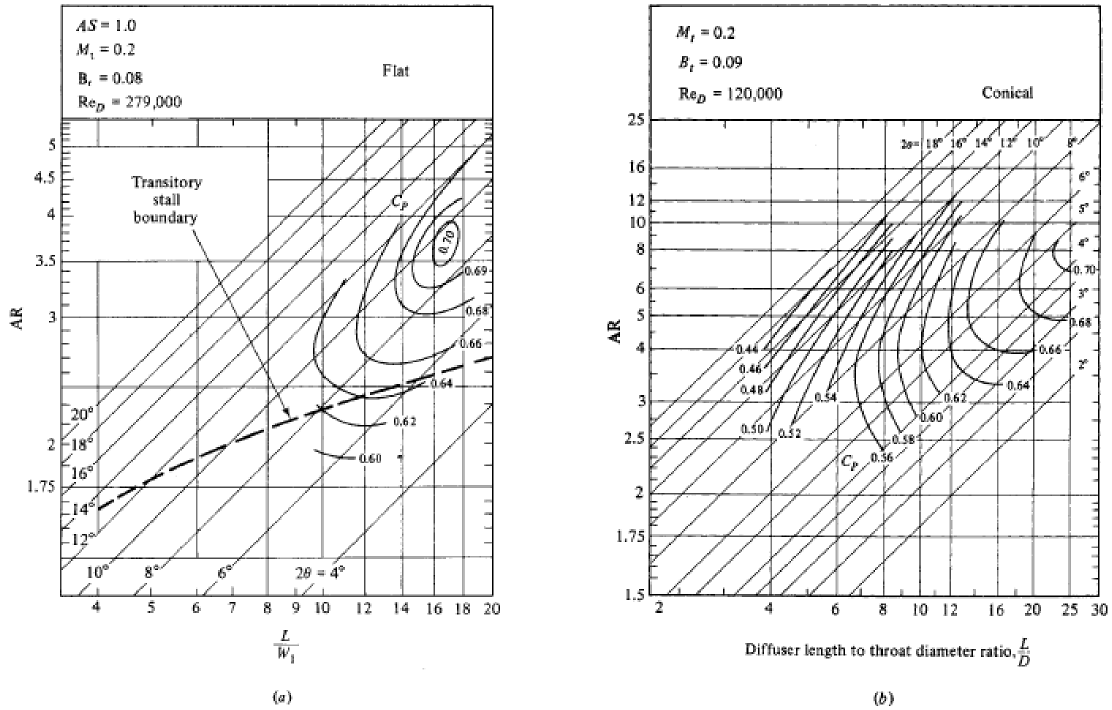

(a)

(b)

Fig 4.4 Performance maps for (a) flatwalled, (b) conical diffusers at similar operating conditions [41]

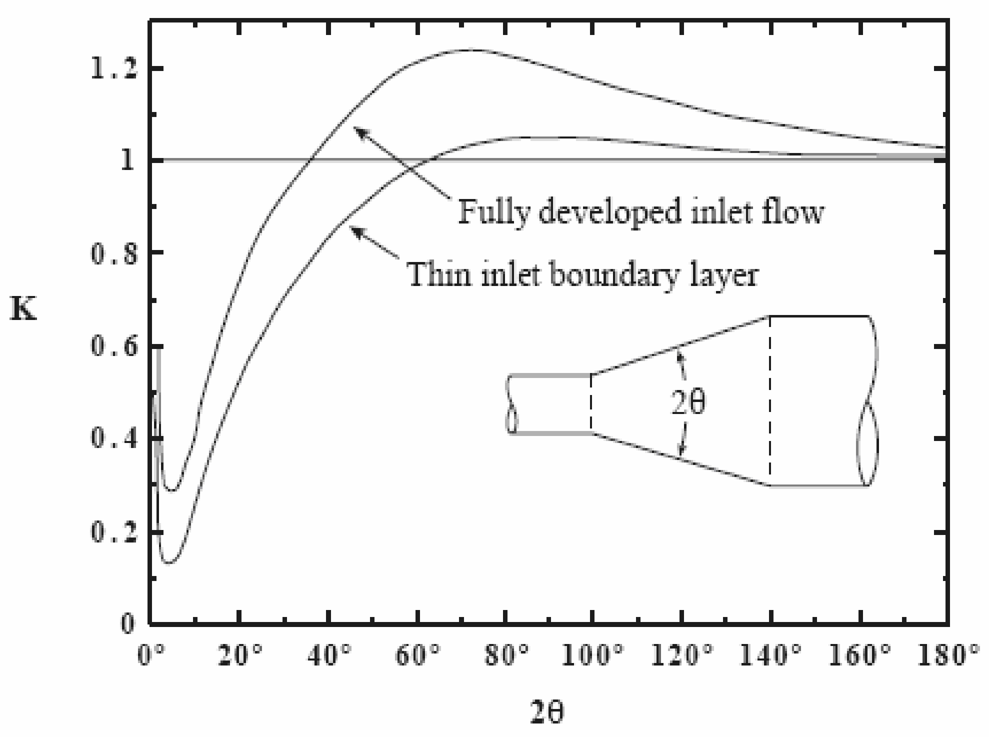

Fig 4.5 Loss coefficient as a function of 2θ for conical diffuser [41]

In order to achieve the best pump performance the diffuser element has to be designed for highest possible flow directing capability. To estimate the possible flow directing capability of diffuser element available information for macroscopic internal flow systems with circular cross-section was used. The pressure drop in an internal flow system is usually given as the loss coefficient, *K,* which is related to the pressure drop, Δp, by [26, 41, 42]

$$\Delta p = K. (½). (\rho v^2_{exit}) \qquad 4.3$$

where ρ is the fluid density and v_{exit} is the mean velocity upstream. For the complete diffuser element it is more practical to relate the pressure drop to the velocity in the narrowest cross-section, the throat, as

$$\Delta p =\xi. (½). (\rho v^2_{throat)} \qquad 4.4$$

where ξ is the pressure loss coefficient and v_{throat} is the mean velocity in the throat. The relation between ξ and K is given by:

$$\xi = K. (A_{throat} / A_{exit})^2 \qquad 4.5$$

To optimize the efficiency of the diffuser element the ratio η should be maximized. To achieve this entrance region of the diffuser should be rounded. The outlet should be sharp. In our design diffuser/nozzle was designed based on trial and error method due to lack of published data in the flow velocity regime in which the pump operates and also the flow is pulsating due to the diaphragm oscillations. The diffuser elements have rounded inlet and sharp outlet in the diffuser direction in order to reduce the pressure loss, hence major pressure loss occurs in the bulk diffuser region. For stationary flow total diffuser loss coefficient is 0.2 ~ 1.In the nozzle direction the inlet is sharp and outlet is rounded. As a result of this the pressure loss across inlet and bulk nozzle region is less than that across rounded outlet. So the nozzle performance is independent of element geometry as long as basic design is followed and the total nozzle loss coefficient is 1. The nozzle/diffuser efficiency (η_{nd}) is defined by

$$\eta_{nd} = \xi_n / \xi_d \qquad 4.6$$

Hence the pump performance depends on the diffuser performance of the diffuser/nozzle element.

4.4 Pump Calculation

As discussed in previous section, the pressure drop across a diffuser and nozzle elements are given by:

$$\Delta P_{diffuser} = (½).\ (\rho.\upsilon_d^2).\ \xi_d \qquad 4.7$$

$$\Delta P_{nozzle} = (½).\ (\rho.\upsilon_n^2).\ \xi_n \qquad 4.8$$

where ρ is the fluid density and υ_d and υ_n are the fluid flow velocities in the narrowest part (the throat) of the diffuser and the nozzle, respectively. υ_d and υ_n are assumed to be constant across the cross section. ξ_d and ξ_n are pressure-loss coefficients of the diffuser and the nozzle, respectively.

The volume flows in the diffuser and nozzle are

$$\Phi_d = A_d\, \upsilon_d \qquad 4.9$$

$$\Phi_n = A_n\, \upsilon_n \qquad 4.10$$

where A_d and A_n are the throat cross-sectional area of the diffuser and nozzle respectively.

From above equations,

$$\Phi_d = A_d \cdot (2 / \rho)^{½} \cdot (\Delta P_d / \xi_d)^{½} \qquad 4.11$$

$$\Phi_n = A_n \cdot (2 / \rho)^{½} \cdot (\Delta P_n / \xi_n)^{½} \qquad 4.12$$

We have used the same element as diffuser and nozzle that gives the same cross-sectional throat area: $A_d = A_n = A$. If the inlet and outlet pressure, P_i and P_o, can both be neglected compared to the chamber pressure, P_c,the volume flows in the diffuser and nozzle direction can be written as

$$\Phi_d = C / (\xi_d)^{½} \qquad 4.13$$

$$\Phi_n = C / (\xi_n)^{½} \qquad 4.14$$

where $C = A(2P_c / \rho)^{½}$.

As the pump diaphragm is moved up and down by the piezoelectric actuator the motion of the diaphragm can be approximated by a sine wave and the chamber volume variation is

$$V_c = V_x \sin(\omega t) \qquad 4.15$$

If pump operates at a frequency f then $\omega = 2\pi ft$ where V_x is the volume variation amplitude. This gives a net chamber volume flow of

$$\Phi_i - \Phi_o = dV_c/dt = V_x\, \omega \cos(\omega t) \qquad 4.16$$

where Φ_i is the volume flow into the chamber through the inlet and Φ_o is the volume flow out of the chamber through the outlet.

SUPPLY MODE

During the supply mode the chamber volume increases, $dV_c /dt > 0$, which gives a net flow into the chamber with the inlet element acting as a diffuser and the outlet element acting as a nozzle. This gives inlet and outlet flows of

$$\Phi_i = \Phi_d = C / (\xi_d)^{½}$$

$$\Phi_o = - \Phi_n = - C / (\xi_n)^{½}$$

This yields a net chamber flow of

$$\Phi_i - \Phi_o = C\{ (1 / (\xi_d)^{½}) + (1 / (\xi_n)^{½})\} = V_x \omega \cos(\omega t)$$

which gives

$$C = \{ V_x \omega \cos(\omega t) \} / \{ (1 / (\xi_d)^{½}) + (1 / (\xi_n)^{½})\} \qquad 4.17$$

The supply mode outlet flow is

$$\Phi_s = - \Phi_n = - C / (\xi_n)^{½} \qquad 4.18$$

which with the expression for C yields

$$\Phi_s = - V_x \omega \cos(\omega t) / [1 + (\xi_n / \xi_d)^{½}] \qquad 4.19$$

PUMP MODE

During the pump mode the chamber volume decreases, $dV_c /dt < 0$ which gives a net flow out of the chamber with the inlet element acting as a nozzle and the outlet element acting as a diffuser. This gives inlet and outlet flows of

$$\Phi_i = - \Phi_n = - C / (\xi_n)^{½}$$

$$\Phi_o = \Phi_d = C / (\xi_d)^{½}$$

So the net chamber flow is

$$\Phi_o - \Phi_i = C\{ (1 / (\xi_d)^{½}) + (1 / (\xi_n)^{½})\} = V_x \omega \cos(\omega t)$$

So the pump-mode outlet flow rate is

$$\Phi_p = - C / (\xi_d)^{½}$$

$$= \{- V_x \omega \cos(\omega t) / [(1 / (\xi_d)^{½}) + (1 / (\xi_n)^{½})]\} / (\xi_d)^{½} \qquad 4.20$$

PUMPED VOLUME

If the pressure-loss coefficients are assumed to be constant throughout the pump cycle, the total pumped volume during one complete pump stroke is

$$V_o = {}_0\int^{T/2} \Phi_s + {}_{T/2}\int^{T} \Phi_p$$

$$= - \{V_x / [1 + (\xi_n / \xi_d)^{1/2}]\} \ {}_0\int^{T/2} \omega \cos(\omega t)\, dt \ - \ \{V_x / [1 + (\xi_d / \xi_n)^{1/2}]\} \ {}_{T/2}\int^{T} \omega \cos(\omega t)\, dt$$

$$V_o = 2V_x\{[(\eta_{nd})^{1/2} - 1] / [(\eta_{nd})^{1/2} + 1]\} \qquad 4.21$$

where $\eta_{nd} = \xi_n / \xi_d$.

4.5 Basic Dosing Properties

The basic dosing properties are quiet similar among the various micropump designs and concepts. Fig 4.6 shows the typical pump flow rate as a function of actuation frequency and influence of varying outlet overpressure. The pump rate linearly increases with the operation frequency up to certain corner frequency and after that it drops due to insufficient relaxation and other secondary effects depending on the micropump design. The pump flow rate decreases as the outlet overpressure is increased and after certain value the operation stops. The influence of varying backpressure poses a limit to the dosing accuracy of the pump. Use of high force actuation can extend the maximum backpressure values beyond the operational values needed for certain application. In order to realize the self priming and bubble tolerant pump the minimum values of compression ratio, β ratio of stroke volume to the pump chamber volume, for liquid pump is in the order of 10^{-6} and 10^{-2} for gas pumps. In summary the micropump must be able to deliver accurate quantity of dose at desired rate, biocompatible [39].

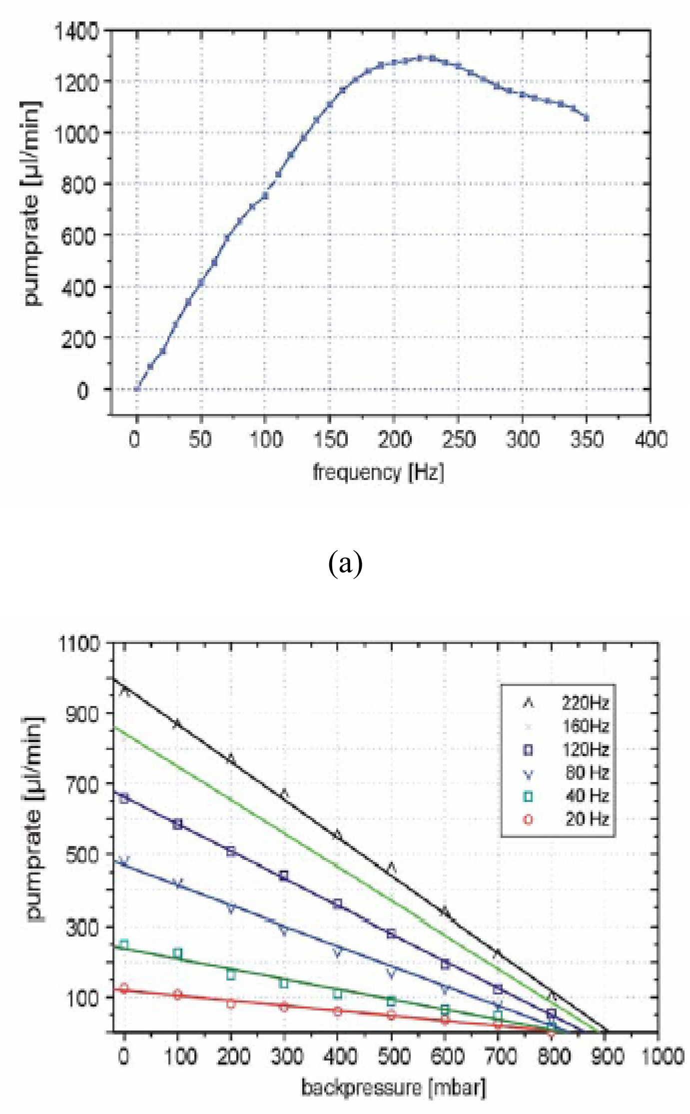

(a)

(b)

Fig 4.6 Typical dosing property of micro diaphragm pump: pump rate as a function of (a) frequency, (b) applied outlet backpressure with water as medium [39]

4.6 Pump Design

The pump prototype is made by assembling the pump chamber, nozzle/diffuser and the actuator together. The pump chamber is designed by making a rectangular cavity of dimension 34mm x 5 mm x 0.3mm in a stainless steel plate and closing the cavity with thin (0.15 mm) aluminum diaphragm. The dimensions of the pump chamber are chosen by considering the actuator design, displacement of the cap and the compressibility (β) requirement for the liquid pump. The diaphragm is bonded with the center portion of the actuator cap. Diaphragm oscillates by applying alternating excitation voltage to the actuator. The diffuser/nozzle elements are bonded to the other side of the pump chamber using epoxy. In order to hold the pump chamber stable it is bonded from the sides to the actuator steel blocks using epoxy. Fig 4.7 shows the schematic diagram of the designed pump.

The diffuser/nozzle element design follows the basic principle shown in Fig 4.4. The throat diameter is 0.635 mm and the outlet diameter is 0.767 mm. The area ratio, (D_{exit}/D_{throat}) is 1.46. The value of (L/D_{throat}) is 10. Based on these parameters using the Fig 4.4, 4.5 and equation 4.5 the values of diffuser and nozzle loss coefficients were calculated and found to be $\xi_d=0.41$ and $\xi_n=1$ respectively. Hence the nozzle/diffuser efficiency can be calculated using equation 4.6, as $\eta_{nd}=2.43$.

The FEM analysis was used to calculate the displacement of pump diaphragm and stress on it. The FEM analysis was done with driving voltage of 8.5 V. Fig 4.8 shows the admittance plot for the pump design shown in Fig 4.7 and the resonance frequency was found to be 2.075 kHz. The displacement of the center point of the diaphragm is shown in Fig 4.9. Fig 4.10 shows the stress acting on the pump diaphragm. From FEM analysis it was found that due to bonding of diaphragm and cap the displacement magnitude of the actuator cap decreased. Fig 4.11 shows the design of the fabricated pump. The sequence of the change in pump chamber volume due to the actuator cap and hence pump diaphragm movement is shown in Fig 4.12.

The pump stroke volume (ΔV) for the diaphragm displacement of 0.18 μm was calculated to be 0.0347 mm^3. The pump chamber volume (V) was 51 mm^3. The compression ratio, $\beta = \Delta V / V$, is 6.8E-4 which is more than the minimum value required for the liquid micropump (10^{-6}). The pump flow rate was 18.4 μl/min for operating voltage of 8.5 V and frequency of 60 Hz. The pump flowrate can be increased either by increasing driving voltage or the frequency.

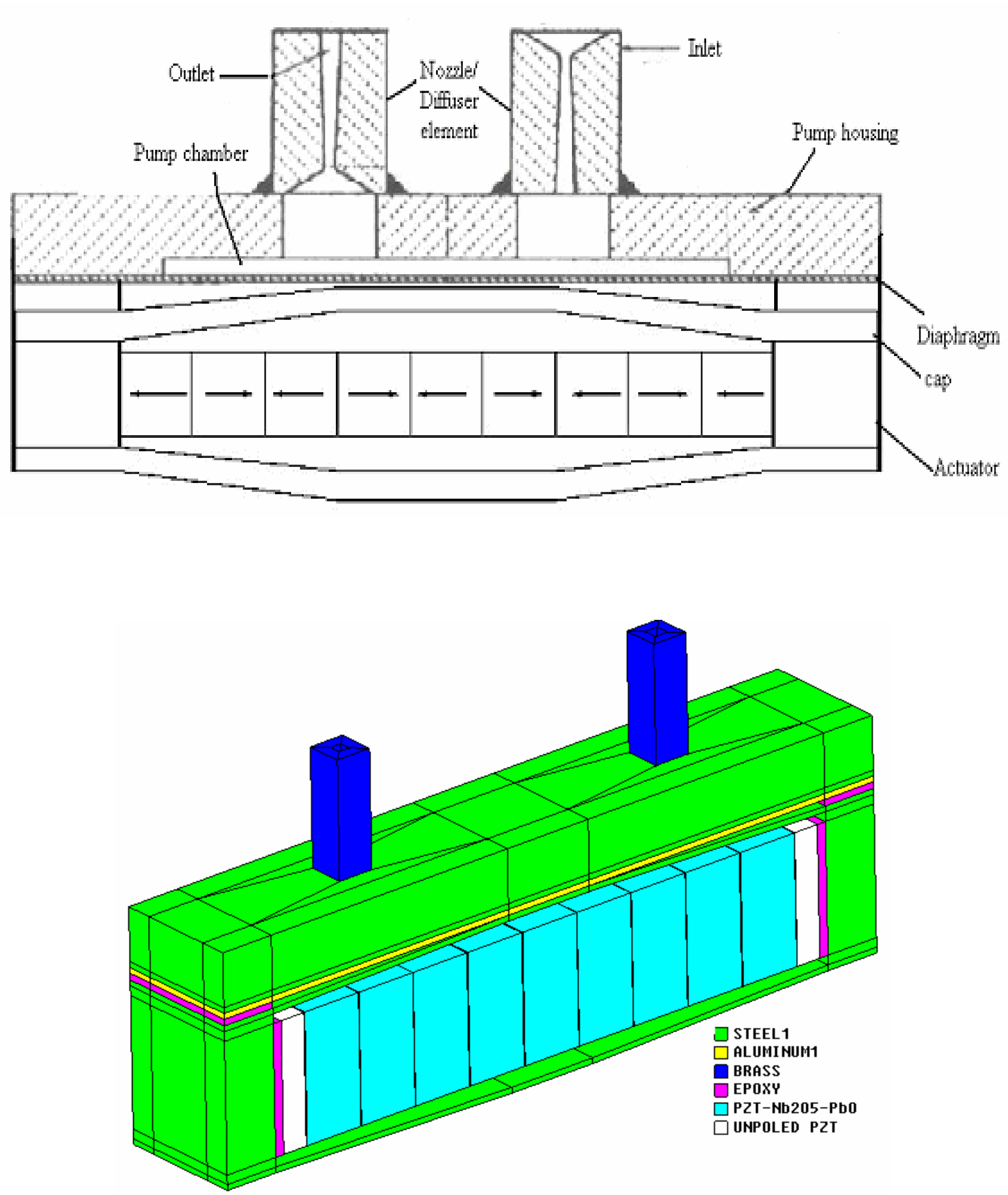

Fig 4.7 Schematic diagram of the designed pump

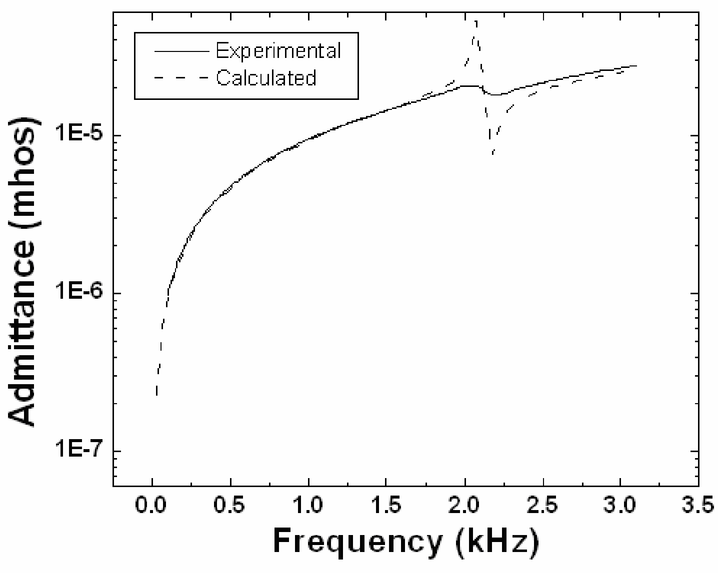

Fig 4.8 Admittance plot for the pump design shown in Fig 4.7

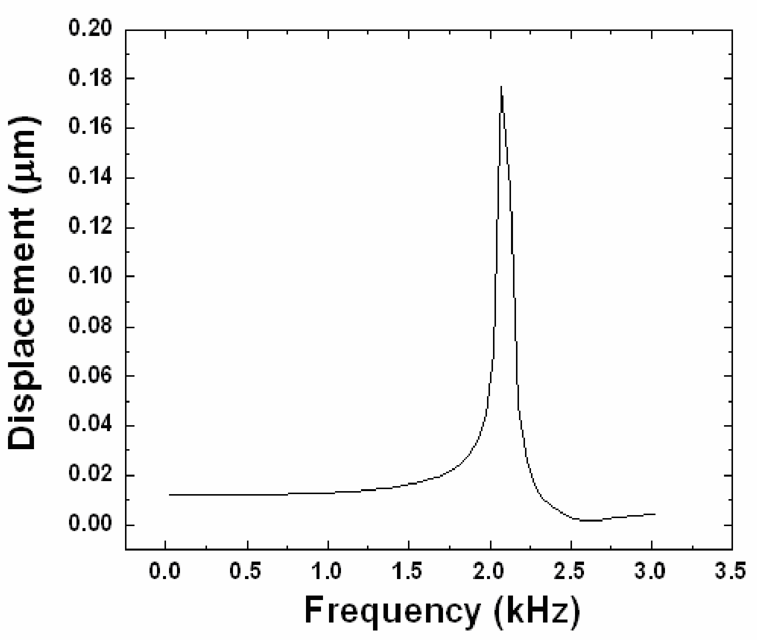

Fig 4.9 Displacement of the center node of the pump diaphragm

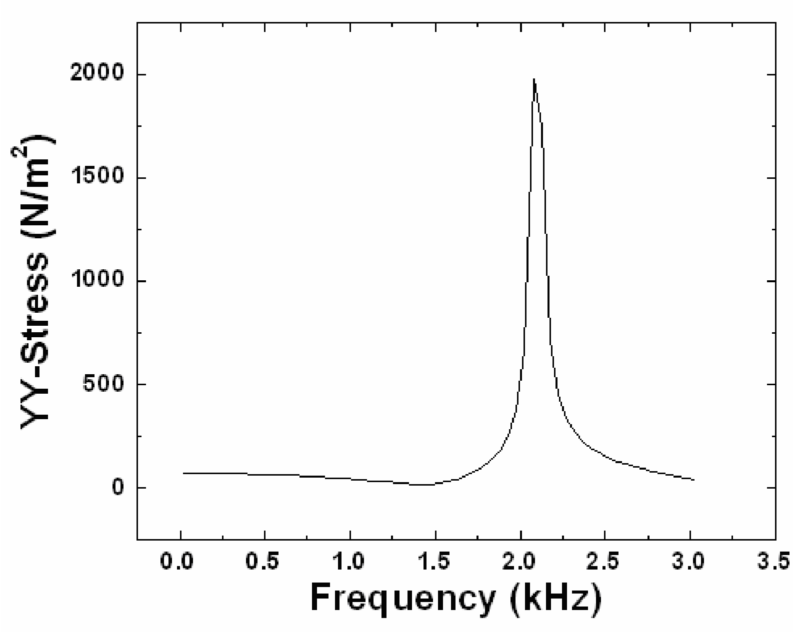

Fig 4.10 Stress on center node of the pump diaphragm

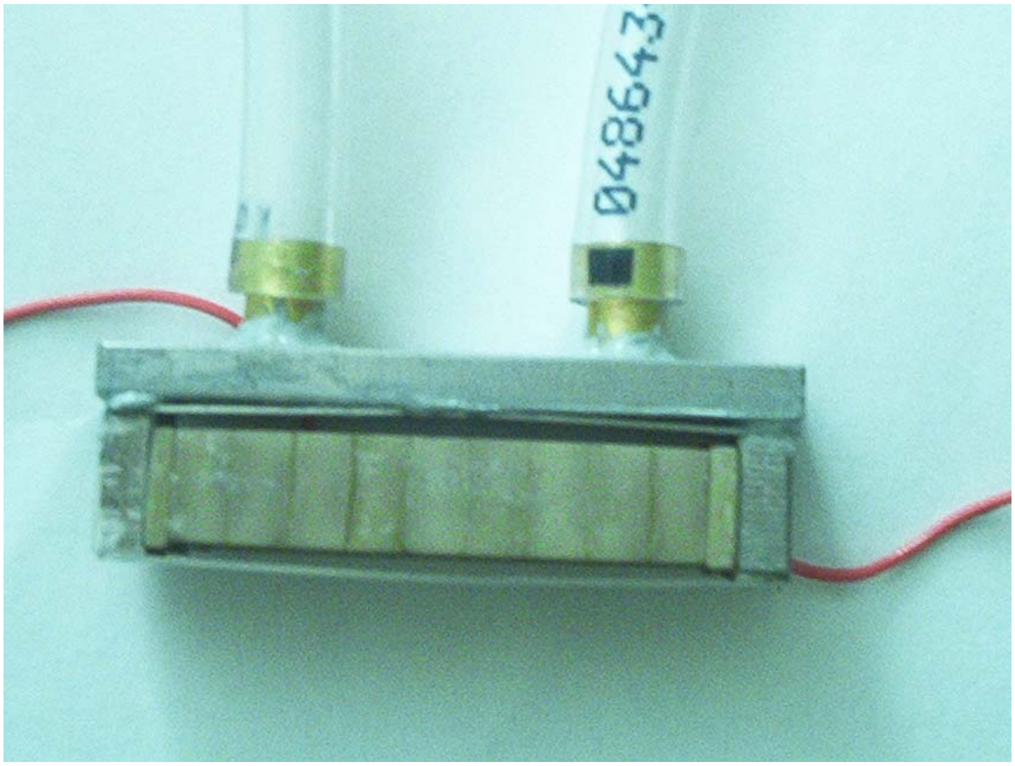

Fig 4.11 Fabricated pump design

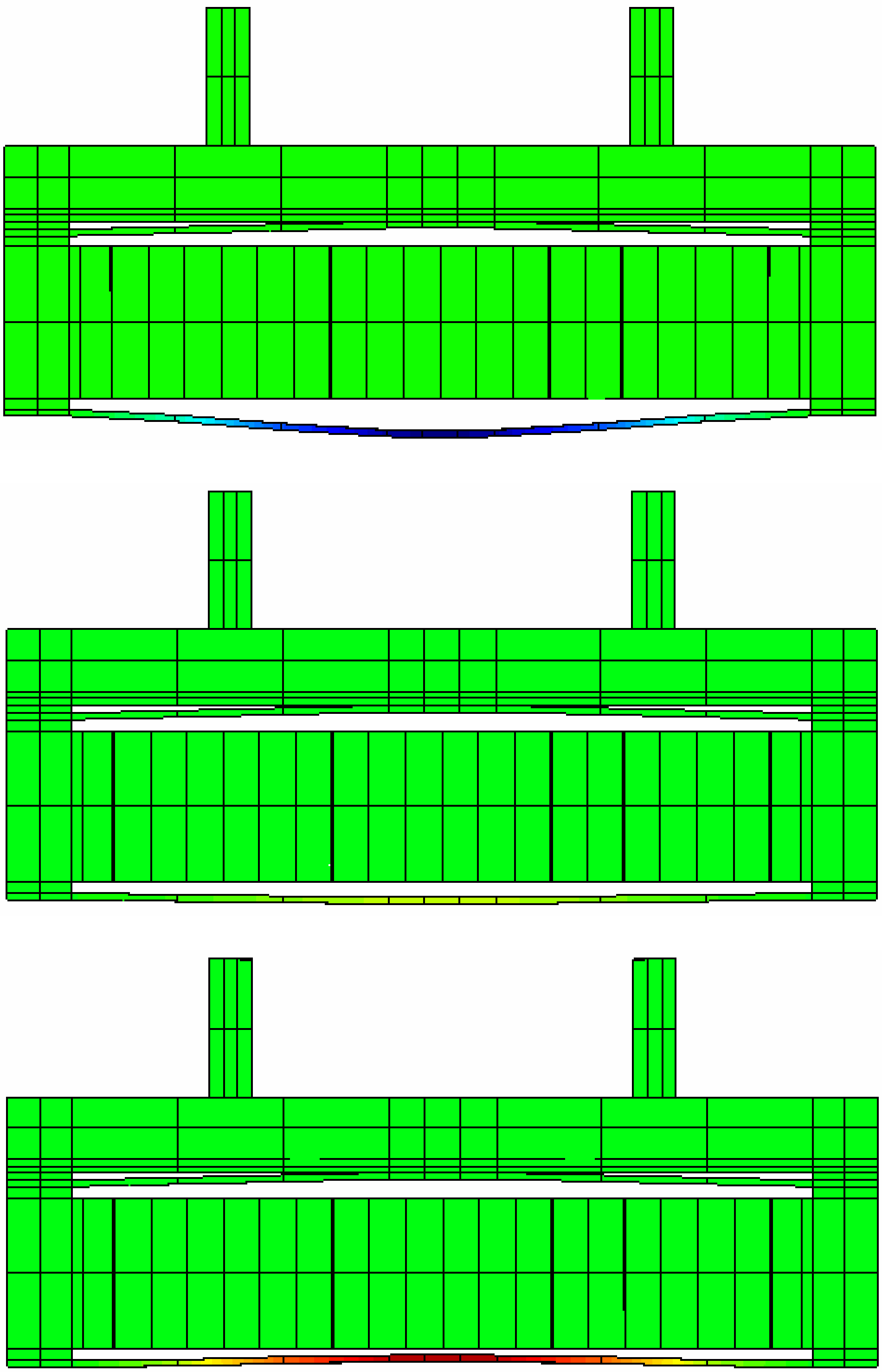

Fig 4.12 Displacement of the pump diaphragm

The fabricated pump was driven in the frequency range of 0.1 - 2 kHz at various applied voltages, however no pumping was found to occur. It is expected that this is due the following problems (i) bonding between the diaphragm and metal cap was not efficient restricting the generated pressure in the chamber and (ii) calculated dimensions of the diffuser/nozzle elements were not optimum restricting the transport of the pressure from inlet to outlet.

CHAPTER 5

ACTUATOR- HIGH FREQUENCY OPERATION

5.1 Introduction

The design described in the thesis can also be extended to fabricate an actuator operating in the high frequency range of few ten's of kHz depending upon the size. The advantage of the design presented here is that it provides large displacement through flextension of the metal caps at low driving voltages leading to an excellent drive and control system. Another objective of this work was to make a design which can produce wide range of blocking force and displacement. As mentioned before the actuator parameters can be varied to obtain the desired performance.

The FEM analysis of the design was carried out using the Atila GiD software (Magsoft Corporation, NY). PZT-5A material was selected as the piezoelectric element. The piezoelectric properties of PZT-5A used in the simulation are listed in Table I. Table II shows the material data for the steel cap used for the optimization of the ceramic and cap dimensions. All the simulations were performed on the 3-D models with high mesh density under an excitation field of 3V/mm.

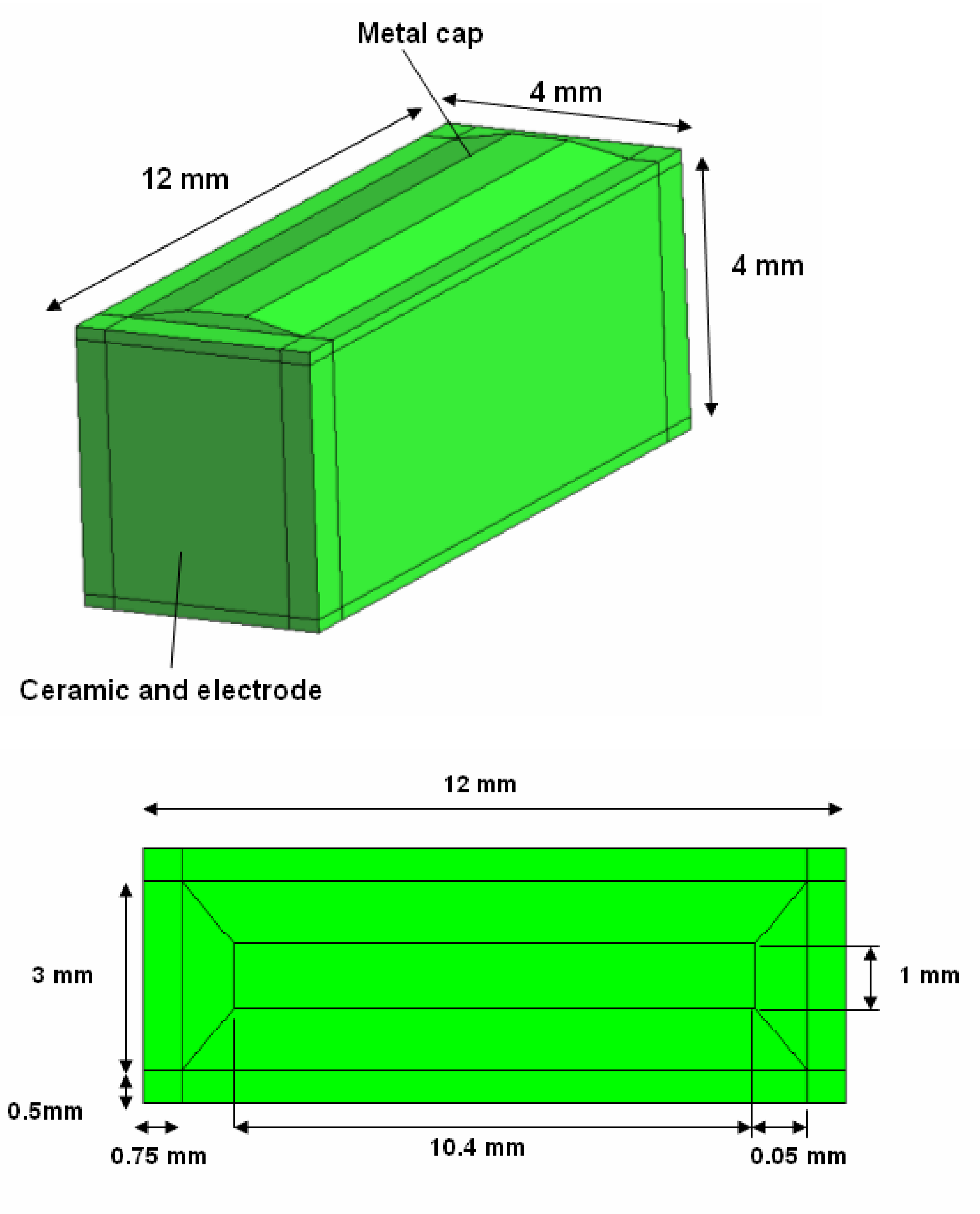

Fig 5.1 Schematic diagram of the actuator and metal cap

Table 5.1 Data for the ceramic material-PZT5A (in standard MKS units)

Properties	**Magnitude**	**Properties**	**Magnitude**
S_{11}^{E}	16.4×10^{-12}	D_{15}	584×10^{-12}
S_{12}^{E}	$- 5.74 \times 10^{-12}$	D_{31}	-171×10^{-12}
S_{13}^{E}	$- 7.22 \times 10^{-12}$	D_{33}	374×10^{-12}
S_{33}^{E}	18.8×10^{-12}	$\varepsilon_{11}^{T}/\varepsilon_{o}$	1730
S_{44}^{E}	47.5×10^{-12}	$\varepsilon_{33}^{T}/\varepsilon_{o}$	1700
$\tan\delta_{m}$	0.013	$\tan\delta_{d}$	0.02

Table 5.2 Data for the metal cap material- Steel

Properties	**Magnitude**
Young’s Modulus	215×10^{9} kg/m^{2}
Poisson’s ratio	0.33
Density	7.9 gm/cm^{3}

5.2 33-mode Metal-Ceramic Actuator

In this bar type metal-ceramic actuator the piezoelectric bar is poled along the length, and the metal caps are attached to the two opposite major faces. Fig 5.1 shows the schematic diagram of the actuator design. The metal caps are rectangular in shape and have a rectangular cavity at the center. The electrodes are printed on the square faces of the piezoelectric bar and the ceramic is poled along the length direction. The electrical connections on the 33-mode metal-ceramic actuator can be easily made by soldering or gluing the wires on the electroded faces. Since the metal-cap is perpendicular to the direction of the applied field it gives advantage in terms of isolating the wire connections.

Flextensional vibration mode depends on various design parameters and material used for cap such as length (L_b), width (W_b) and thickness (T_b) of the ceramic bar; length and width of the metal cap (l_c and w_c), height of cavity (h_c) and thickness of the metal cap (t_c). To exemplify, Fig 5.1 shows the values for the various parameters that provide flextensional mode in vicinity of the longitudinal mode. It can be seen from this figure that there are various parameters that can affect the resonance characteristics. Table III summarizes the various coefficients of the optimized configuration using FEM simulation. The height of cavity and cap material has significant effect on the vibration characteristics; hence these factors were studied in detail to clearly delineate the functional dependence.

In this FEM study, simulations were performed on a single layer ceramic bar. However, the configuration shown in Fig.5.1can be easily fabricated using the commonly available multilayer actuators which consist of several layers of ceramics stacked in the poling direction.

5.3 Optimization of Ceramic Aspect Ratio

The computed admittance plot in a wide frequency range of 1 kHz – 550 kHz for the actuator dimensions described in Table 5.3 and Fig 5.1 is shown in Fig 5.2. Several resonance peaks were observed in this frequency range. The resonance peak observed at 123 kHz corresponds to fundamental longitudinal mode and that at 140 kHz corresponds to fundamental flextensional mode. The second longitudinal resonance was observed at 348 kHz. A small peak at 318 kHz was found to be a bending mode along the poling direction. Various higher order resonance peaks were found in the high frequency region indication the coupling between various dimensions. It can be seen in this figure that the flextensional mode for the chosen dimensions couples with the longitudinal mode and has frequency interval exactly in between the resonance and antiresonance of the longitudinal mode. The aspect ratio of the ceramic (length/width or length/thickness) for this case was 3. Various aspect ratio’s were investigated and it was found that for the aspect ratios lower than 3 or higher than 3 the bending mode shifted towards higher frequencies or become very weak. Thus, the aspect ratio of 3 provides the best coupling. The advantage of having flextensional mode in the vicinity of the longitudinal mode is that a large displacement could be obtained over a wider frequency range.

Figures 5.3 (a) and (b) shows the displacement of the actuator at 123 kHz and 140 kHz. The displacement magnitude at 140 kHz is higher than that at 123 kHz. At

140 kHz, the maximum displacement is observed in the center region of the cap while no displacement was found for ceramic bar. On the other hand, at 123 kHz corresponding to longitudinal mode high displacement is found both in ceramic bar and metal caps, and the maximum displacement occurs in the electroded region of the ceramic Comparing the magnitude of the total displacement, it can be seen that the displacement at 123 kHz is about half of that at 140 kHz.

Fig 5.4 shows the variation of the total displacement as a function of the frequency in the frequency range of 100 – 170 kHz at the center node of the metal cap. It can be seen from this figure that the displacement has a high magnitude over a wide frequency range with the maxima occurring at the resonance corresponding to the flextensional vibration mode with magnitude of around 0.48 μm. The discontinuities occurring at the maximum displacement points may be due to some spurious in the resonance spectrum which were not visible on the admittance frequency plots.

Table 5.3 List of design parameters for actuator design shown in Fig 5.1

L_b(mm)	W_b(mm)	T_b(mm)	l_c(mm)	w_c(mm)	t_c(mm	h_c(mm)	Metal cap material	Ceramic material
12	4	4	10.4	1	0.2	0.2	Steel	PZT 5A

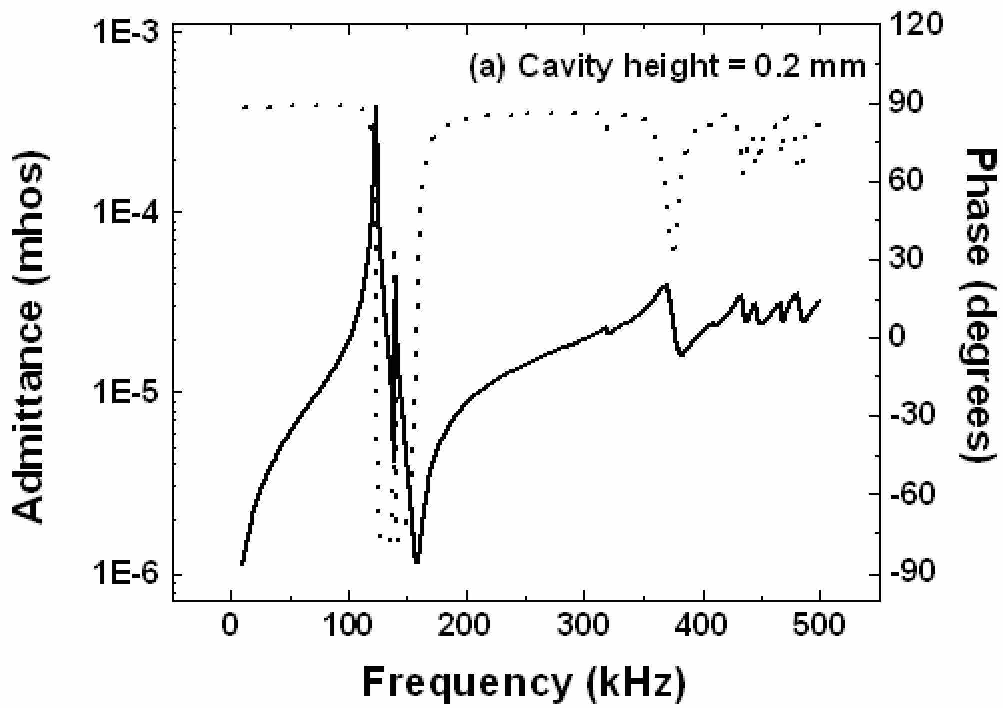

Fig 5.2 Admittance plot for actuator design shown in Fig 5.1

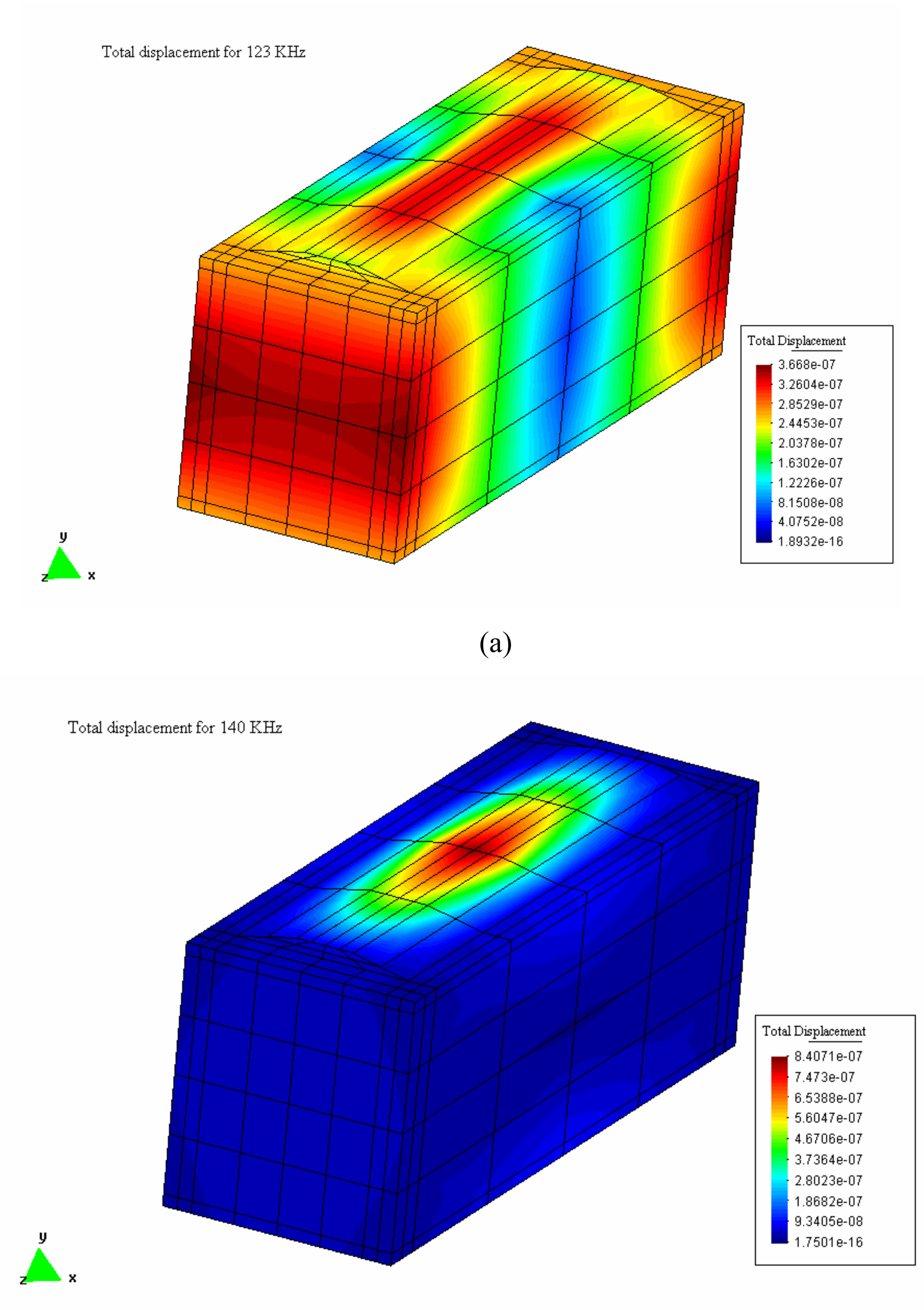

(a)

(b)

Fig 5.3 Displacement of the actuator at (a) 123 kHz, (b) 140 kHz

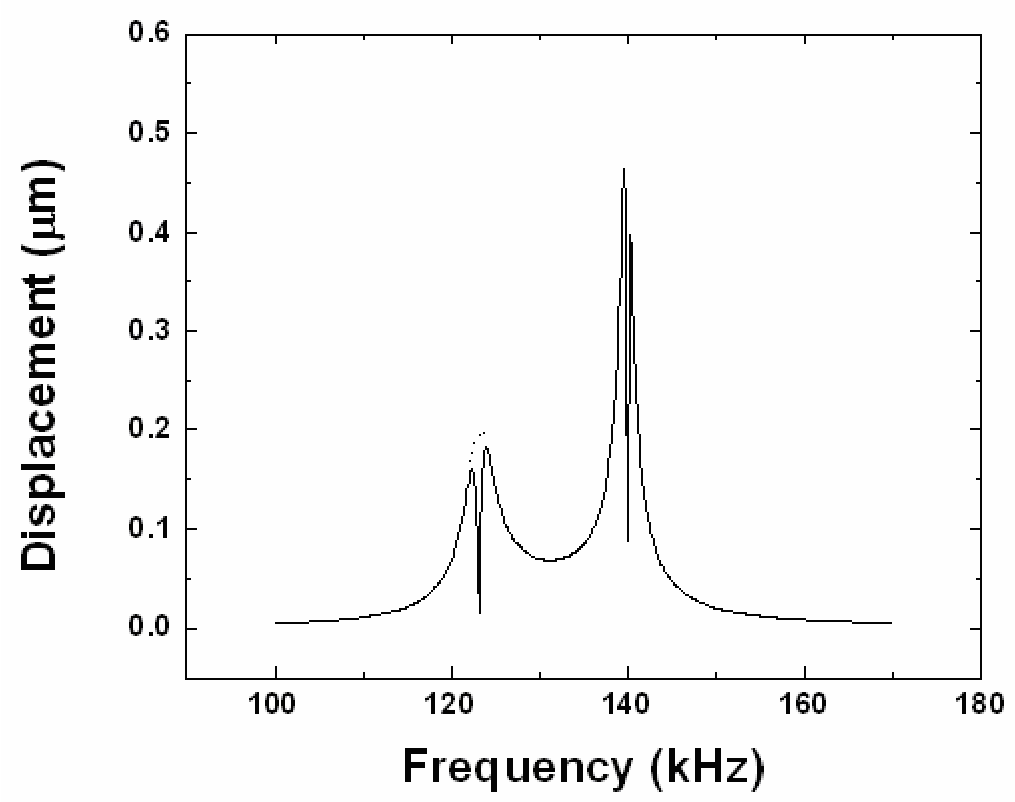

Fig 5.4 Displacement at the center node of the cap

As mentioned before, the flextensional vibration mode is very sensitive to the design parameters, metal cap and ceramic material. Fig 5.5 shows the affect of the length of the ceramic bar on the vibration modes. It can be seen that as the length of the ceramic bar increases (while keeping width and thickness constant) the fundamental longitudinal vibration mode shifts to the lower frequency while the flextensional mode even though stays at the same frequency diminishes with increasing length.

Fig 5.6 shows the affect of change in the dimension of the ceramic upon the admittance. In this figure the calculation was done for the case of 26.4 mm and 40.8 mm. For both the cases the aspect ratio for the ceramic and all the other dimensions were kept in the same ratio as shown in Fig 5.1, i.e. the dimensions in Fig 5.6(a) were all multiplied with 2.2 and that in Fig 5.6(b) were multiplied with 3.4. In all the simulations the driving field of 3 V/mm was kept constant. Clearly it can be seen in this figure that whole admittance curve moves towards the lower frequency in a fixed ratio. The longitudinal mode resonance frequency for the case of ceramic length with 12 mm occurs at 123 kHz, while for the other two cases of 26.4 mm and 40.8 mm occurs at 56 kHz and 36.2 kHz respectively. This change in the resonance frequency is approximately in the same ratio of 2.2 and 3.4 as expected for this mode. The resonance frequency of the flextensional mode also changes in the same ratio.

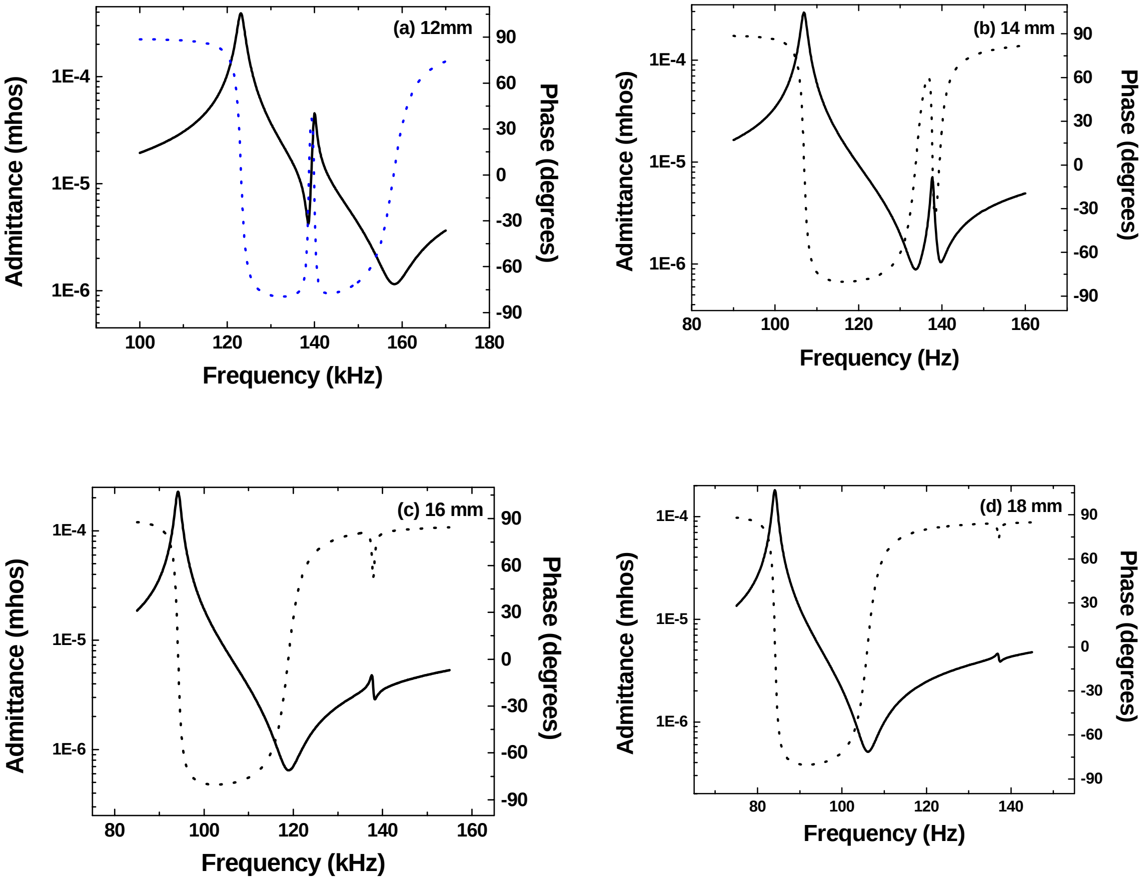

Fig 5.5 Effect of actuator length on vibration mode

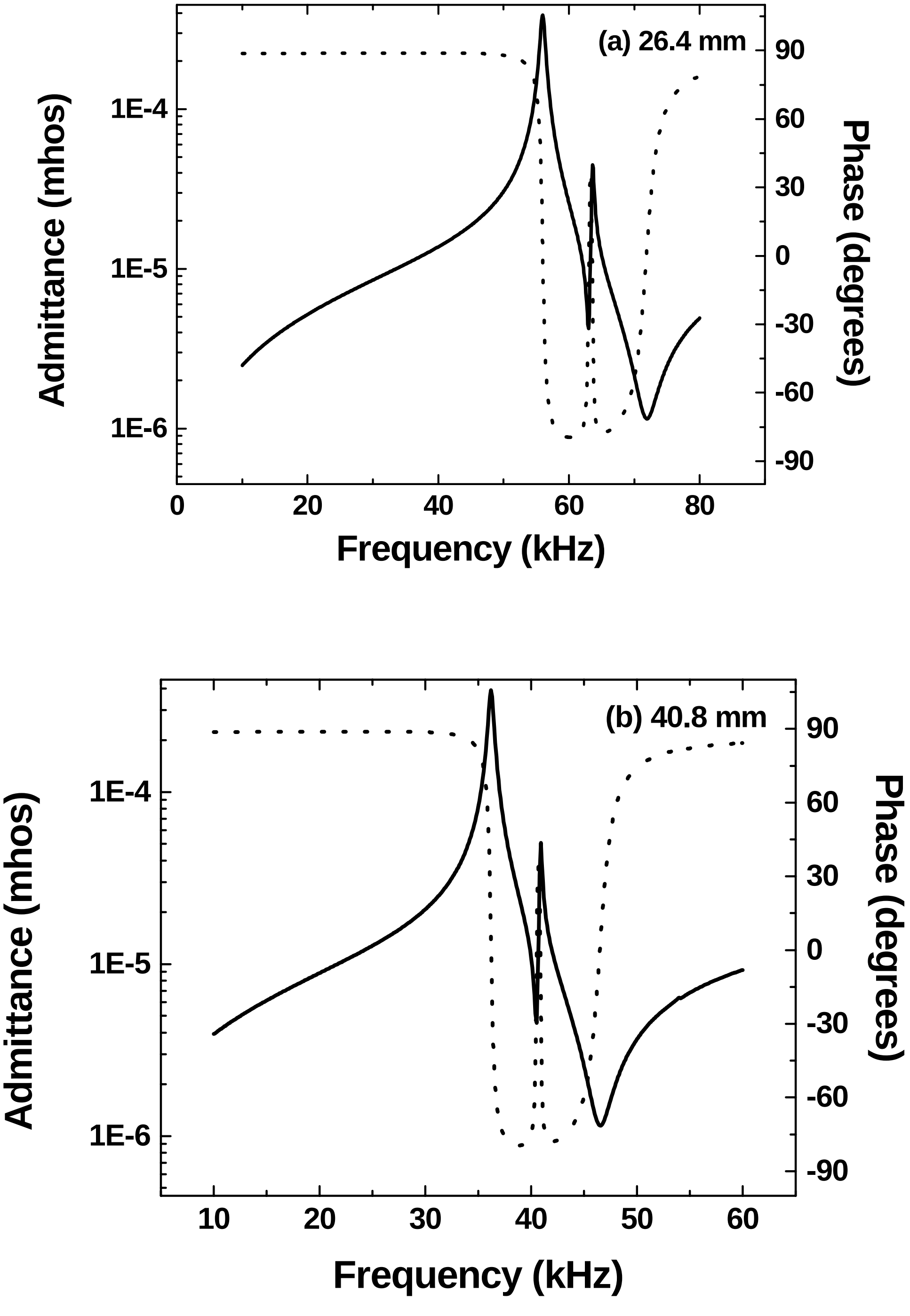

Fig 5.6 Effect of change in ceramic dimensions on admittance curve

Fig 5.7 shows the affect of the cavity depth on the admittance curve. Comparing with Fig 5.2 it can be seen that as the cavity depth increases the flextensional mode peak is shifted towards the higher frequency. This result is significant as it provides a method for shifting the flextensional mode to desired frequency range.

5.4 Effect of Metal Cap Material

The metal cap material is known to affect the admittance spectrum significantly. Fig 5.8 shows the admittance spectrum for metal cap material of brass and titanium having the dimensions shown in Fig 5.1.Comparing the results of Fig 5.8 with that of Fig 5.2 (metal cap material = steel) significant differences can be seen. For the case of brass metal cap, two peaks corresponding to first order and second order flextensional mode can be seen at 100.6 and 130.8 kHz.

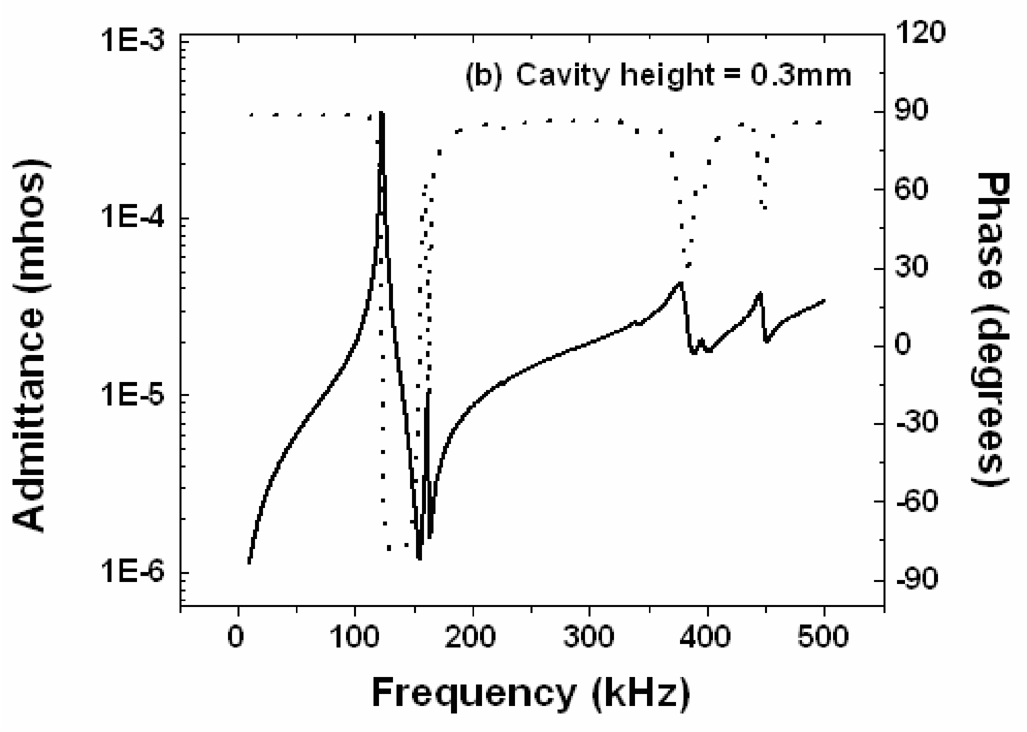

Fig 5.7 Effect of the cavity depth on the admittance curve

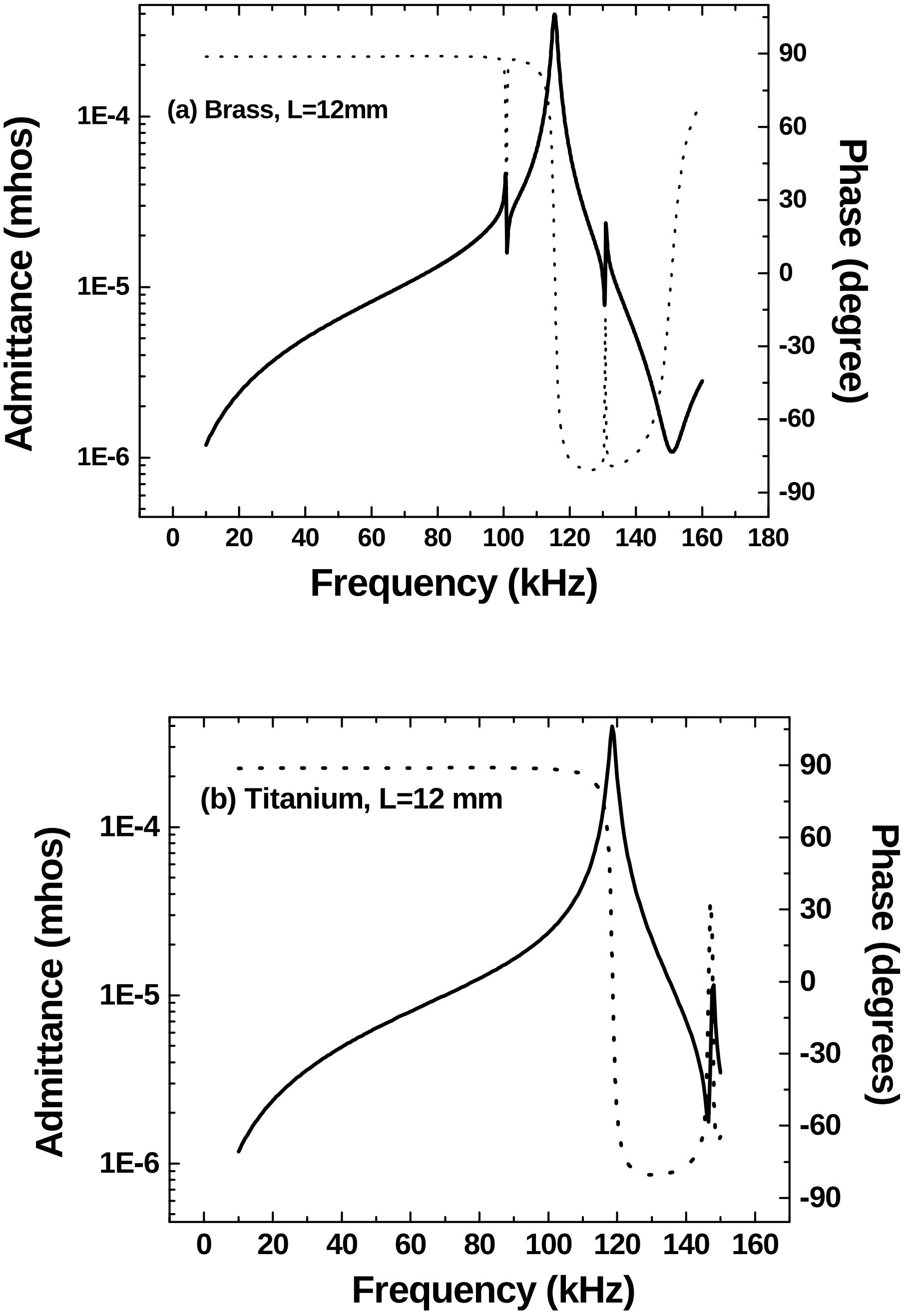

Fig 5.8 Effect of metal cap material on admittance curve

Fig 5.9 shows the displacement variation at the two flextensional modes for the actuator with brass metal caps. The two peaks at 130.8 kHz can be clearly seen and in this case the displacement is not maximum at the center of the metal cap. In the case of the titanium the admittance curve is similar to that of steel but the flextensional mode occurs at higher frequency. From these results two important results can be clearly pointed out; (1) The flextensional mode occurs at lower frequency as the density of the cap material is increased, and (2) For the higher density material, the second order flextensional mode appears in the vicinity of the first order.

The results of Fig 5.8 are quite interesting for designing the wide range high displacement – high blocking force actuator. The modified design for actuator having dimensions 30 x 10 x 10 mm^3 with brass metal cap is used to lower the frequency range. It can be noted that the aspect ratio of 3 was maintained in the design. Fig 5.10 shows the admittance spectrum for this modified design with various cavity heights. In all the simulations the driving field of 3 V/mm was kept constant. Interestingly, the two flextensional modes of the brass can be seen to come closer and finally merge with increasing cavity heights. A high displacement along the top of metal cap is obtained in this case. One of the significant advantages of this design is that high displacement is obtained over a wide surface area.

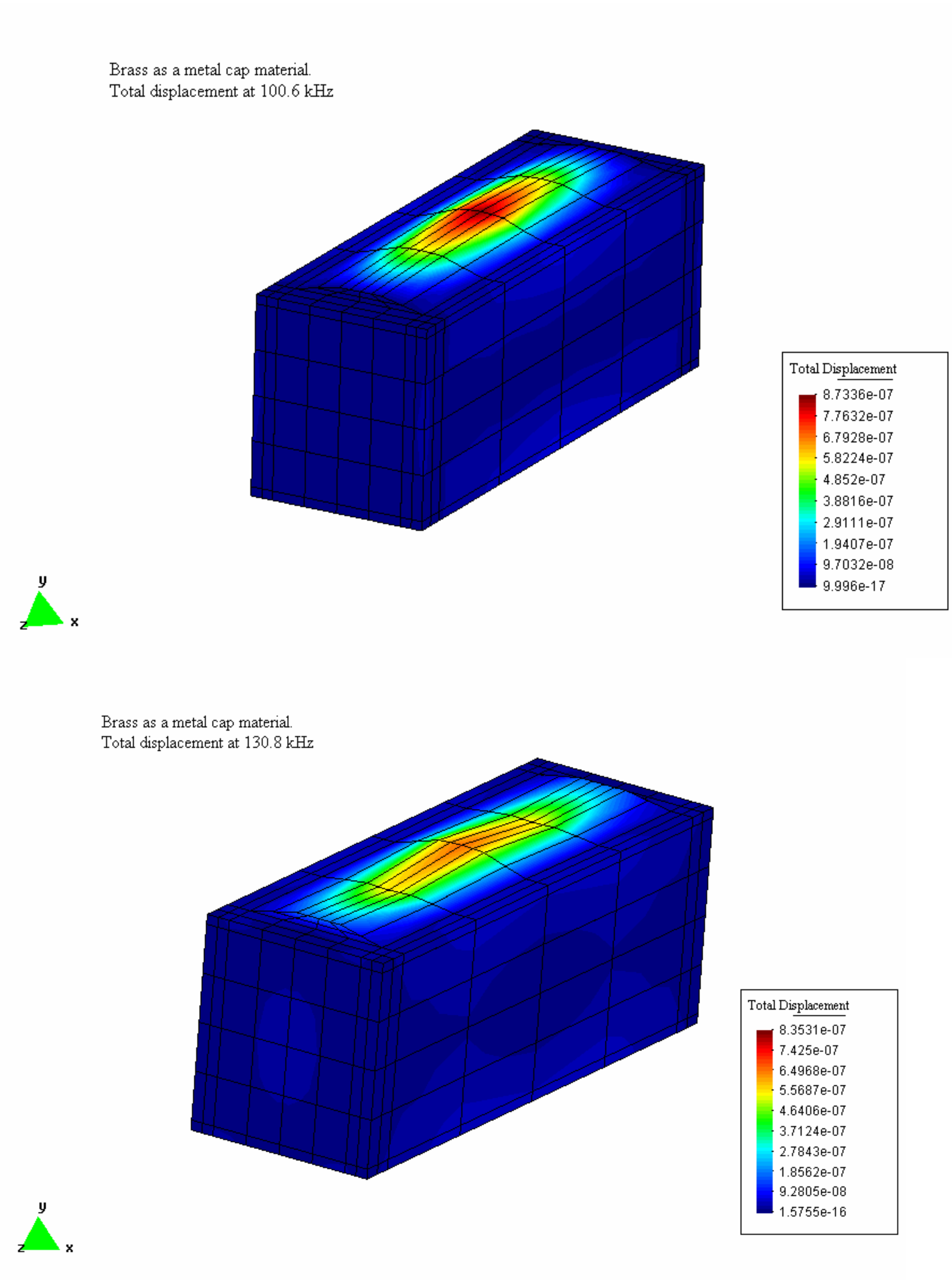

Fig 5.9 Displacement variation at the two flextensional modes for the actuator with brass metal caps

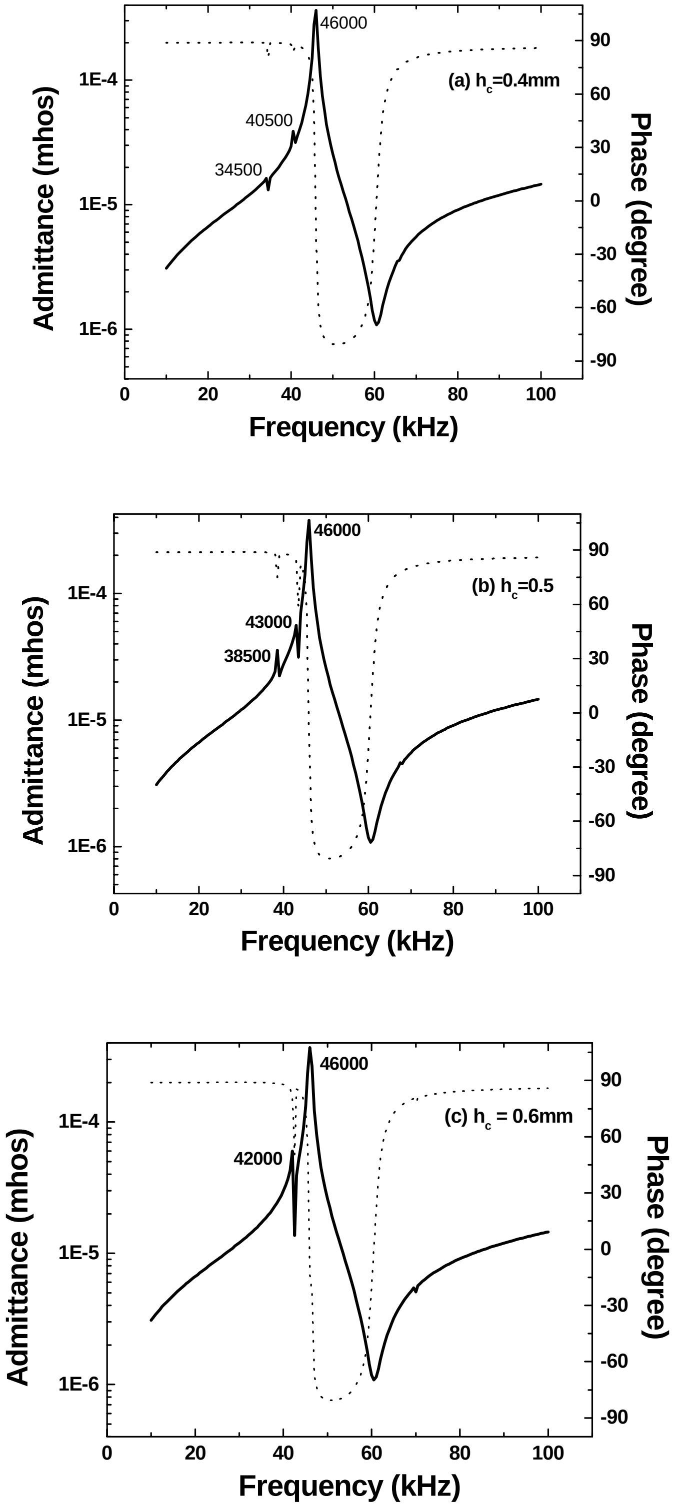

Fig 5.10 Admittance curve of modified 10x10x30 mm^3 design for different cavity depth

5.5 Analytical Model

A simple 2-dimensional model can be used to calculate the displacement produced in the composite actuator. This model is based on the approach developed by the Fernandez et al [44]. Fig 5.11 shows the parameters for the ceramic and metal cap where the subscripts "b" denotes the ceramic bar and the subscripts "c" denotes the cavity. L_t denotes the total length of the cavity. In the flextensional mode, the total displacement in the actuator at the center of the cap (x) is sum of the transversal expansion of the ceramic plus the change of the cavity depth due to longitudinal shrinkage:

$$x = 2\Delta h_c + \Delta h \qquad 5.1$$

where Δh is the change in the cavity depth and Δh is the transversal expansion of the ceramic under applied electric field E:

$$\Delta h \ = -d_{31} E L_b \qquad 5.2$$

where L_b is the length of the ceramic bar. It should be noted here that the magnitude of transverse piezoelectric constant, d_{31}, is negative so Δh corresponds to expansion of the ceramic. The cavity depth change can be expressed as:

$$h_c + \Delta h_c = \left[l^2 - \left\{ \frac{\left(L_t\left(1 - d_{33}E\right) - L_c\right)}{2} \right\}^2 \right]^{1/2} \qquad 5.3$$

where l is the lateral wall of the metal cap, L_t is the total length of the metal cap and L_c is the length of the top part of the metal cap. Combining the Eq. 5.2 and 5.3 with 5.1, the displacement of the actuator can be expressed as:

$$x = 2\left[1^2 - \left\{\frac{\left(L_t\left(1 - d_{33}E\right) - L_c\right)}{2}\right\}^2\right]^{1/2} - 2h_c - d_{31}EL_b \qquad 5.4$$

Substituting the values from the Table III and Fig 5.1 for the actuator parameters, the displacement was found to be 9.1 nm for a field of 3 V/mm. This magnitude is static value which will be amplified at the resonance. It is evident from Equation 5.4 that the displacement can be enhanced by decreasing the top part of cap and increasing the lateral wall of cap. This displacement magnitude can be enhanced by using the multilayer structure. Hence, for a 6 layer structure a displacement of 23.8 nm can be obtained for the same field level of 3V/mm.

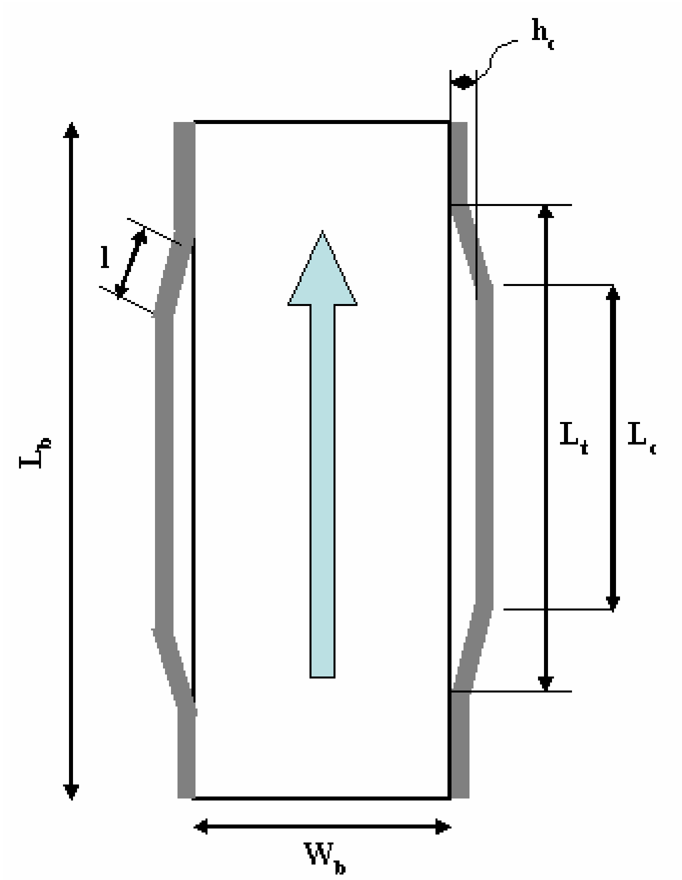

Fig 5.11 Parameters for the ceramic and metal

CHAPTER 6

FUTURE WORK

Some important extensions of this work are as follows:

(1) Actuator design should be improved by changing the metal cap material and dimensions to further lower the resonance frequency.

(2) Actuator design should be tested under high field-high stress condition to realize the effects of practical operating conditions.

(3) Analytical model for the actuator needs to be developed.

(4) Pump should be redesigned to overcome the problems. In this aspect, a detailed computational modeling using ANSYS would be very helpful and should be attempted in future studies.

(5) Pump with check valves may also be fabricated to provide cheaper version of the micropump using the actuator design proposed in this thesis.

REFERENCES

[1] B. Culshaw, “Smart structures and materials”, Artech House, 1996, Boston.

[2] J. D’Cruz, “Active suppression of aircraft panel vibration with piezoelectric strain actuators”, Journal of Intelligent Material Systems and Structures, vol. 1, 1990, 4-25.

[3] V.Giurgiutiu, “Active material induced strain actuation of aeroelastic vibration control”, Shock and Vibration Digest, vol.32, 2000, 355-368.

[4] J. Moor, R. Spangler, K. Lazarus, D. Henderson, “Buffetload alleviation using distributed piezoelectric actuators”, Proceedings of ASME Aerospace division, vol. AD52, ASME,1996,485-490.

[5] R. Clark, C. Fuller, “Experiments on active control of structurally radiated sound using multiple piezoceramic actuators”, Journal of Acoustical Society of America, vol.91, 3313-3320.

[6] C. Fuller, C. Hansen, S. Snyder, “Active control of structurally radiated noise using piezoceramic actuators”, Proceedings of Inter-Noise, 1989, 509-512.

[7] C. Niezrecki, H. Cudney, “Feasibility of using piezoelectric actuators to control launch vehicle acoustics and structural vibrations”, Proceedings of SPIE, 1990, 5-9.

[8] F. Austin, W. Van Nostrand,“Shape control of an adaptive wing for transonic drag reduction”Smart Structures and Materials, vol. 2447, 1995, 45-55.

[9] G. Washington, “Smart aperture antennas”, Smart Materials and Structures, vol.5, 1996, 801-805.

[10] L. Pack, R. Joslin, “Overview of active flow control at NASA Langley Research Center”, SPIE Smart Structures and Materials, vol.3326, 1998, 202-213.

[11] V. Varadan, V. Varadan, “Smart electronics and MEMS for aerospace structures”, SPIE Micromachined Devices and Components, vol.2642, 166-172.

[12] F. Crawley, “Intelligent structures for aerospace: A technology overview and assessment” AIAA Journal, vol.32, 1689-1699.

[13] G. Haertling, “Rainbow ceramics-A new type of ultra high displacement actuators”, American Ceramic Society Bulletin, vol.73, 1994b, 93-96.

[14] B. Barron, G. Li, G. Haertling, “Temperature dependent characteristics of Cerambow actuators”, IEEE International Symposium on Application of Ferroelectrics, Part I, IEEE vol.96CH35948, 1996, 305-308.

[15] R. Bryant, “LaRC^{TM}-SI: A soluble aromatic polyimide”, High Performance Polymers, vol.8, 1996, 607-615.

[16] A. Moskalik, D. Brei, “Quasistatic behavior of individual C-Block piezoelectric actuators”, Journal of Intelligent Material Systems and Structures. Vol.8, 571-587.

[17] N. Herakovic, “Die untersuchung der nutzung des piezoeffektor zur ansteurung fluide ventille”, Ph.D dissertation,1996.

[18] L. Mauck, C. Lynch,“Piezoelectric hydraulic pump”, SPIE Smart Structures and Materials 1999: Smart Structures and Integrated Systems, vol.3668, 844-852.

[19] J.Tressler, W. Cao, K,Uchino, R.E. Newnham, “ Finite-element Analysis of Cymbal type Flextensional Transducer”, IEEE, Transactions on Ultrasonics, Ferroelectrics and Frequency control, 45, 5 ,1998, 1363-1369.

[20] A.Dogan and R. E. Newnham, “Metal-electroactive ceramic composite transducer”, U.S. Patent No. 5, 729, 077, 1998.

[21] A. Dogan, K. Uchino, and R. E. Newnham, “Composite piezoelectric transducers with truncated conical endcaps ‘Cymbals’”, IEEE Trans. Ultrason. Ferroelec. Freq. Cont., 44, 1997, 597 – 605.

[22] Burlington Instruments, “The technology behind Burlington Inchworm systems”, Burlington Instruments, 1998.

[23] “Piezoelectric Ceramics: Principles and Applications”, APC International Ltd.2002.

[24] H.T.G. van Lintel, F.C.M van de Pl, S. Bouwstra,“A piezoelectric micropump based on micromachining of silicon”, Sensors and Actuators, 15, 1998, 153-167.

[25] R. Zengerle, S. Kluge, M. Richter, A. Richte,“A bidirectional silicon micropump”, Proceedings of the MEMS, 1995, 19-24.

[26] E.Stemme, G.Stemme, “A valveless diffuser nozzle-based fluid pump”, Sensors and Actuators A, 39, 1993, 154-167.

[27] J. Smits, “Piezoelectric micropump with three valves working peristaltically”, Sensors and Actuators A, 21-23, 1990, 203-206.

[28] D. Harrison, K. Seiler, A. Manz, Z. Fan, “Chemical analysis and electrophoresis systems integrated on glass and silicon chips”, Tech. Dig. IEEE Solid-State Sensors and Actuators Workshop, 1992, 110-113.

[29] S. Bart, L. Tavrow, M. Mehregany, J. Larig, “Microfabricated electrohydrodynamic pumps”, Sensors and Actuators A, 21-23, 1990, 193-197.

[30] W. Spencer, W. Corbett, L. Dominguez, B. Shafer, “An electronically controlled piezoelectric insulin pump and valves”, IEEE Trans. Sonics Ultrason., 25, 1978, 153-156.

[31] H.King, R.E.Aubert, W.H.Herman, “Global Burden of Diabetes, 1995-2025 Prevalence, numerical estimates and projections”,Diabetes Care, 21,1998,1414-1431.

[32] Z. Wan, D. Wu, D. Cruz, A. Lazarev,“Piezoelectric micropump for drug delivery”, 2001.

[33] B. Jaffe, W. Cook, H. Jaffe, “Piezoelectric ceramics”, Academic Press, 1971, p.148.

[34] J. Nye, “Physical properties of crystals, their representation by tensors and matrices”, Clarendon Press, 1957.

[35] A.J. Moulson and J.M.Herbert, “Electroceramics”, John-Wiley & Sons Ltd., 2003, 71-82,339-406.

[36] K.Uchino, “Ferroelectric Devices”, Marcell Dekker Inc. 2000, 4, 61-63,145-196.

[37] C.Jullian,“Investigations of polarization switching over broad time and field domains in various ferroelectrics”, thesis, 2002.

[38] P.Laoratanakul, “Design and characterization of piezoelectric transformers for high power applications”, Ph.D. thesis, 2002.

[39] P.Woias, “Micropump-past, progress and future prospects”, Sensors and Actuators B 105, 2005, 28-38.

[40] A.Olsson, G.Stemme, E.Stemme, “Valve-less planar fluid pump with two pumps chambers”, Sensors and Actuators, A 46-47, 1995, 549-556.

[41] F.M.White, “Fluid Mechanics”, McGraw Hill Book Company, 1986, 332-350.

[42] A. Olsson, G.Stemme,E.Stemme, “Numerical and experimental studies of flat-walled diffuser elements for valveless micropumps”, Sensors and Actuators, 84, 2000, 165-175.

[43] C.Niezrecki, D.Brei, S.Balakrishnan,A.Moskalik, “Piezoelectric Actuation: State of the Art”, The Shock and Vibration Digest , July 2001,269-280.

[44] R.Letty, F.Claeyssen, F.Barillot, and N.Lhermet, “Amplified Piezoelectric Actuators for aerospace applications”, AMAS Workshop on Smart Materials and Structures SMART’), September 2-5, 2003, 51–62.

[45] D.P.Garg1, M.A.Zikry and G.L.Anderson, “Current and potential future researchActivities in adaptive structures: an ARO perspective”, Institute of physics publishing, smart mater. struct., 10,2001, 610–623.

[46] T.Zhang, Q.Wang, “Valveless piezoelectric micropump for fuel delivery in direct methanol fuel cell (DMFC) devices”, Journal of Power Sources 140, 2005, 72–80.

[47] S. Priya, S. Ural, H. W. Kim, K. Uchino and T. Ezaki, “Multilayered Unipoled Piezoelectric Transformers”, Jpn. J. Appl. Phys., 43,2004, 3503 – 3510.

[48] J. F. Fernandez, A. Dogan, J. T. Fielding, K. Uchino, and R. E. Newnham, "Tailoring the performance of ceramic-metal piezocomposite actuators, 'cymbals'", Sensors and Actuators A, 65, 1998, 228 – 237.

[49] J. Zhang, W. J. Hughes, P. Bouchilloux, R. Meyer, Jr., K. Uchino, and R. E. Newnham, "A class V Flextensional Transducer: The Cymbal", Ultrasonics, 37,1999, 387 – 393.

BIOGRAPHICAL INFORMATION

Miteshkumar S Joshi was born on 19th February in Bardoli, India. He did his secondary and higher secondary studies from M.B.Vamdot High School, Bardoli. He has been awarded a 'gold medal' for getting first place in secondary board examinations. He did his Bachelor's of Chemical Engineering from S.P.University, V.V.Nagar, India. Currently he is pursuing Masters of Science in Materials Science and Engineering at University of Texas at Arlington and working under the guidance of Dr. Shashank Priya. His research interests are high power piezoelectric materials and devices. He is currently working on high power actuators and developing a micropump for drug delivery application. He wants to get industrial experience while working in the field of piezoelecrics.